

Collider Implications of Kaluza-Klein Excitations of the Gluons

D.A. Dicus,^{(a)*} C.D. McMullen^{(b)†} and S. Nandi^{(b)‡}

^(a) *Center for Particle Physics, University of Texas,
Austin, Texas 78712, USA*

^(b) *Department of Physics, Oklahoma State University
Stillwater, OK 74078, USA*

Abstract

We consider an asymmetric string compactification scenario in which the SM gauge bosons can propagate into one TeV^{-1} -size extra compact dimension. These gauge bosons have associated KK excitations that present additional contributions to the SM processes. We calculate the effects that the KK excitations of the gluons, g^* 's, have on multijet final state production in proton-proton collisions at the Large Hadron Collider energy. In the case of dijet final states with very high p_T , the KK signal due to the exchanges of the g^* 's is several factors greater than the SM background for compactification scales as high as about 7 TeV. The high- p_T effect is not as dramatic for the direct production of a single on-shell g^* , which subsequently decays into $q\bar{q}$ pairs, where the KK signal significantly exceeds the SM three-jet background for compactification scales up to about 3 TeV. We also present our results for the four-jet final state signal from the direct production of two on-shell g^* 's.

*email: phbd057@utxvms.cc.utexas.edu

†email: mcmulle@okstate.edu

‡email: shaown@osuunx.ucc.okstate.edu

1. Introduction

Recent developments in superstring theory have sparked much interest in scenarios where the string scale is much smaller than the four-dimensional Planck scale [1]. The size of the six extra compact dimensions may be much larger than the inverse Planck scale, giving rise to many new phenomenological possibilities. For n large extra dimensions compactified at the same scale R^{-1} , the size R is related to the four-dimensional Planck scale M_P via the relation

$$M_P^2 = M_\star^{n+2} R^n, \quad (1)$$

where M_\star is the $(4+n)$ -dimensional Planck scale, which is of the order of the string scale. Recently, it was shown that this relation (1) is phenomenologically viable [2] for $n \geq 2$, R can be in the sub-millimeter regime, and the string scale could be fairly close to the electroweak scale, namely, a few tens of a TeV. The gauge hierarchy problem is eliminated since the four-dimensional Planck scale M_P is not a fundamental quantity in this scheme. If all six extra dimensions from the superstring theory are compactified at the same scale, then $1/R$ is about 10 MeV. Thus, if the Standard Model (SM) particles are allowed to propagate into these extra dimensions (the bulk), they will have Kaluza-Klein (KK) excitations with masses at the 10 MeV scale. The non-observation of such KK states up to about a TeV at present high-energy colliders therefore implies, in such scenarios, that all SM particles are confined to a three-dimensional brane (D_3 brane) of the usual three spatial dimensions. These are the key features of the class of models based on the symmetrical compactification proposal of Arkani-Hamed, Dimopoulos, and Dvali (ADD) [2] for solving the hierarchy problem.

It is also possible, however, to devise a model with asymmetrical compactification where SM particles live in a brane which extends into one or more TeV^{-1} -size extra dimensions. The lowest lying KK excitations then have masses at the TeV scale, at the edge of the grasp of present high-energy colliders. Such a scheme has many interesting consequences. For example, it alters the evolution of the gauge couplings from the usual logarithmic to power law behavior [3]. The unification scale can be several orders of magnitude smaller [3], even as low as a few TeV. Recently, an asymmetrical compactification scenario was proposed with two distinct compactification scales [4]: n dimensions of size $R \sim \text{mm}$ and m of size $r \sim \text{TeV}^{-1}$. In particular, we consider the $n = 1$, $m = 5$ case. The scaling relation for this model is [4]

$$M_P^2 = M_\star^3 R = M^8 R r^5. \quad (2)$$

It was shown in Ref. [4] that this model satisfies all of the current astrophysical and cosmological constraints [5]. With $1/R \sim 10^{-3} \text{ eV}$ and $1/r \sim 1 \text{ TeV}$, we get $M \sim 100 \text{ TeV}$ and $M_\star \sim 10^5 \text{ TeV}$. In this scenario, the SM gauge bosons (and perhaps the Higgs boson) can propagate into one of the TeV^{-1} -size extra dimensions, while the SM fermions are confined to the usual D_3 brane. $M \sim 100 \text{ TeV}$ is then consistent

with the unification scale (assuming about a factor of ten uncertainty due to threshold and other effects). The smoking gun signatures of this scenario are deviations from Newton’s law of gravity in the sub-millimeter regime as well as new high- p_T jet physics in high-energy hadron colliders.

Most of the work on the collider phenomenology of extra dimensions [6] has been on the ADD scenario in which only the graviton propagates in the bulk. Hence, the only additional contribution to collider processes stems from the KK excitations of the graviton. The contributions of individual KK modes, with 4D gravitational strength, to collider processes is extremely small. However, the compactification scale μ is so small ($\mu \sim \text{mm}^{-1} \sim 10^{-3} \text{ eV}$) that a very large number of such modes contribute in a TeV-scale collider process, yielding a significant total deviation from the SM results. Studies of various collider processes typically give a bound on the string scale (taken approximately to be the cut-off scale) of about a TeV [6].

The asymmetric scenario, in which SM fields, in addition to gravity, may propagate in one or more extra dimensions of TeV^{-1} -size, will have a more direct effect in high-energy collider processes. Beginning with the original suggestion by Antoniadis [7], some work has also been done for the collider phenomenology of this scenario [8], including the effects on EW precision measurements [9], Drell-Yan processes in hadronic colliders [10], and $\mu^+\mu^-$ pair production in electron-positron colliders [10]. The typical bound is 1–2 TeV for the compactification scale.

In this work, we study the scenario proposed in Ref. [4], in which only the SM gauge bosons (and perhaps the Higgs boson) propagate into one of the TeV^{-1} -size extra dimensions.* More specifically, we study the effects that the KK excitations of the gluons have on multijet production in high-energy hadronic colliders such as the Large Hadron Collider (LHC). We calculate the modifications to the SM cross sections for multijet final states which arise from the direct production and exchanges of KK excitations of the gluons. At the LHC energy, we find substantial deviations from the SM predictions for dijet final states up to a compactification scale of about 7 TeV; whereas for the Tevatron, the KK contribution only exceeds the SM background for small compactification scales ($\lesssim 2.0 \text{ TeV}$). For the direct production of a g^* on-shell at the LHC, which subsequently decays into $q\bar{q}$ pairs, the effect is not as pronounced as the dijet case, but is still significant. We also present the contribution of the production of two on-shell g^* ’s. Our paper is organized as follows. We briefly discuss our formalism in Section 2, and supplement this with additional details in the Appendix. In Section 3, we calculate the effects that the exchanges of g^* ’s have on dijet production and discuss our results and the significance of the SM background. Our analytic expressions for the cross sections for the processes leading to the direct production of one or two on-shell g^* ’s are presented in Sections 4 and 5, respectively; also included are a discussion of our numerical results and, for the single g^* case, comparison to the SM three-jet background. Section 6 contains our conclusions.

*However, our results apply to any compactified string model in which the gluons propagate into one such extra dimension.

2. Formalism

We are interested in tree-level parton subprocesses involving the exchanges or direct production (or both) of KK excitations of gluons. The starting point is the generalization of the 4D SM Lagrangian density to the 5D Lagrangian density. Integration over the fifth dimension then yields the effective 4D Lagrangian density, which includes the usual 4D SM Lagrangian density plus terms involving the KK excitations of the SM gauge fields. These KK terms dictate the possible couplings that the KK excitations can have both with each other and with the SM fields, and provide the Feynman rules for these vertices as well as the KK propagators.

In the model under consideration, the SM gauge bosons can propagate into one large extra compact dimension. The terms in the 5D Lagrangian density relevant to us are (1) the terms involving the contraction of the 5D gluon field strength tensors $F_{MN}^a = \partial_M A_N^a - \partial_N A_M^a - g_5 f^{abc} A_M^b A_N^c$ with 5D indices $M, N \in \{0, 1, \dots, 4\}$, where g_5 is the 5D strong coupling and a, b, c are the usual gluon color indices; and (2) the terms involving the quark fields, which contain a delta function to constrain the SM fermions to the D_3 brane:

$$\mathcal{L}_5 = -\frac{1}{4} F_{MN}^a F^{MNa} + i \bar{q} \gamma^\mu D_\mu q \delta(y). \quad (3)$$

Here, D_μ is the usual 4D covariant derivative, μ, ν are the usual 4D spacetime indices, and the compactified extra dimension coordinate y is related to the radius of the extra dimension r by $y = r\phi$. We consider compactification on a S^1/Z_2 orbifold with the orbifold symmetry, $y \rightarrow -y$ such that $A_\mu^a(x, -y) = A_\mu^a(x, y)$, and impose the gauge choice $A_4^a(x, y) = 0$. This is the unitary gauge. The 5D gluon field $A_\mu^a(x, y)$ can then be Fourier expanded in terms of the compactified dimension y as

$$A_\mu^a(x, y) = \frac{1}{\sqrt{\pi r}} \left[A_{\mu 0}^a(x) + \sum_{n=1}^{\infty} A_{\mu n}^a(x) \cos(n\phi) \right], \quad (4)$$

where the normalization of $A_0^a(x)$ is one-half that of $A_n^a(x)$. When the 5D Lagrangian density is integrated over the extra dimension y , this sum represents a tower of KK excitations $A_{\mu n}^a(x)$ of the gluon field. The $n = 0$ mode gluon is identified with the observed massless gluon of the SM, denoted by g , while the $n > 0$ KK modes, denoted by g_n^* , have masses $m_n = n\mu$ where μ is the compactification scale ($1/r$). It will prove convenient to refer to the $n = 0$ and $n > 0$ modes separately by letting “gluon” or g represent just the $n = 0$ mode, and letting “KK excitation of the gluon” or g^* or g_n^* strictly imply $n > 0$.

The detailed procedure for integrating over the fifth dimension y to obtain, in the effective 4D theory, the factors for the allowed vertices involving KK excitations of the gluons may be found in the Appendix, and lead to the coupling strengths displayed in Fig. 1. Notice that a single g^* can couple to quarks, but not to gluons. Furthermore,

quark-less vertices with N g^* 's only have non-vanishing coupling strengths if the modes n_1, n_2, \dots, n_N of the g^* 's satisfy the relation

$$|n_1 \pm n_2 \pm \dots \pm n_{N-1}| = n_N. \quad (5)$$

Although this relation, Eq. (5), governs the possible vertices, it is not a law expressing 5D momentum conservation for $N \rightarrow M$ processes: For example, a g^* can not decay into gluons at the tree level, although this process is permitted when a quark loop is introduced. Also worth noting are the factors of $\sqrt{2}$, which originate from the different rescaling of the $n = 0$ and $n > 0$ modes, necessary to obtain canonically normalized kinetic energy terms in the effective 4D Lagrangian density [11].

Another difference between the Feynman rules for the g and the g^* lies in the propagator. The g^* propagator is that of a usual massive gauge boson, shown here in the unitary gauge:

$$-i\Delta_{\mu\nu n}^{ab}(p^2) = -i\delta^{ab} \frac{g_{\mu\nu} - \frac{p_\mu p_\nu}{m_n^2}}{p^2 - m_n^2 + im_n \Gamma_n}. \quad (6)$$

At tree-level, the g_n^* decays into $q\bar{q}$ pairs with (total) width $\Gamma_n = 2\alpha_s(Q)m_n^*$.^{*} The decay width can not be neglected because the subprocess energy \sqrt{s} runs up to 14 TeV at the LHC, while we are interested in TeV-scale compactification. For diagrams where a virtual g or g^* exchanges between two quark pairs (*e.g.*, in $q\bar{q} \rightarrow q\bar{q}$), there is the usual diagram with the g propagator in addition to a tower of diagrams with g_n^* propagators, or, equivalently, an effective propagator given by the sum

$$\Delta_{eff}(p^2) = c_0 \Delta_0(p^2) + \sum_{n=1}^{\infty} c_n \Delta_n(p^2). \quad (7)$$

Notice that c_n incorporates the different $q\bar{q}\text{-}g$ and $q\bar{q}\text{-}g_n^*$ vertex factors (*i.e.*, $c_0 = 1$, $c_{n>0} = 2$). This effective propagator can be generalized to the case of arbitrary vertices with appropriate choices of the c_n factors (including setting c_n equal to zero when either vertex is forbidden).

The mass of the g^* also enters into the expression for the cross section via summations over polarization states when external g^* 's are present. For the direct production of g^* 's, the summation of polarization states is given by

$$\sum_{\sigma} \epsilon_{\mu n}^{a*}(k, \sigma) \epsilon_{\nu n}^b(k, \sigma) = \left(-g_{\mu\nu} + \frac{k_\mu k_\nu}{m_n^2} \right) \delta^{ab}. \quad (8)$$

Compare this to the case of external g 's, in which case a projection such as

^{*}We neglect the top quark mass relative to the very heavy g^* .

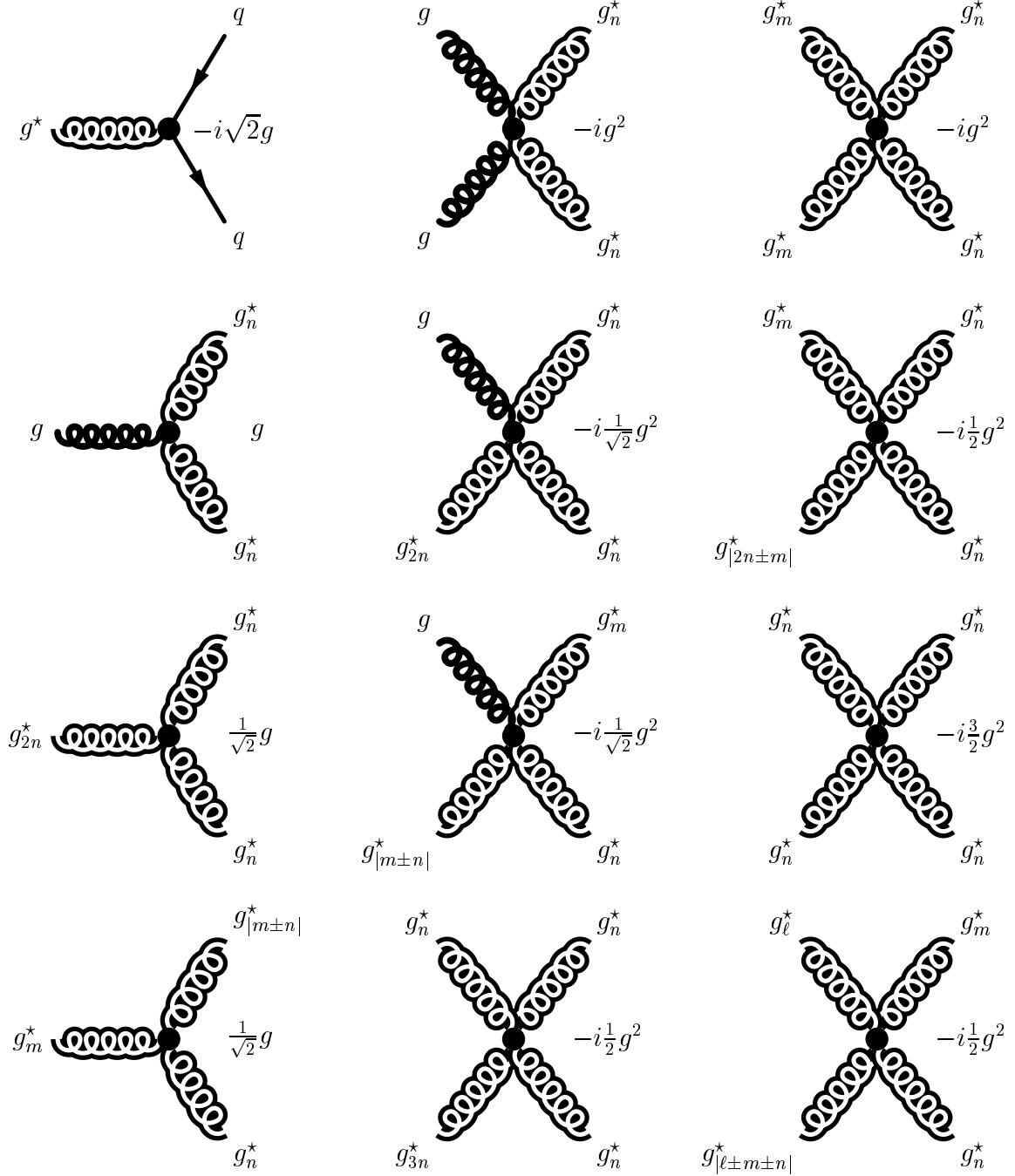


Figure 1: Relative coupling strengths of vertices involving g^* 's. Only the overall factors are shown: The $q\bar{q}g^*$ vertex also involves the SU(3) matrix element and the Dirac γ_μ matrix; triple vertices of g 's and g^* 's also include the usual SU(3) structure functions and the momenta factors; and quadruple vertices of g 's and g^* 's also contain the usual structure function factors as well as the metric tensors $g_{\mu\nu}$. Here, n , m , and ℓ are distinct positive integers ($n \neq m \neq \ell$).

$$\sum_{\sigma} \epsilon_{\mu}^{a*}(k, \sigma) \epsilon_{\nu}^b(k, \sigma) = \left[-g_{\mu\nu} + \frac{(\eta_{\mu} k_{\nu} + \eta_{\nu} k_{\mu})}{(\eta \cdot k)} - \frac{\eta^2 k_{\mu} k_{\nu}}{(\eta \cdot k)^2} \right] \delta^{ab} \quad (9)$$

can be made to eliminate unphysical longitudinal polarization states (and thereby satisfy gauge invariance), for arbitrary four-vector η_{μ} .

3. Dijet Production

For dijet production, all tree-level diagrams are included which do not contain any g^* 's in the final state, since the g^* 's would quickly decay into $q\bar{q}$ pairs, thereby producing additional jets.* Thus, the KK excitations only appear in two-jet diagrams via virtual g^* propagators. The net tree-level effect of the g^* 's on dijet production is the replacement of the SM gluon propagator by an effective KK propagator, wherever five-momentum is conserved. Employing gauge invariance, we drop the second term in Eq. (6) in our analysis of dijet production. It is then convenient to define $D_n(p^2)$ and $D_{\text{eff}}(p^2)$ as

$$\begin{aligned} D_n(p^2) &= \frac{c_n}{p^2 - m_n^2 + im_n \Gamma_n} \\ D_{\text{eff}}(p^2) &= \frac{c_0}{p^2} + \sum_{n=1}^{\infty} c_n D_n(p^2). \end{aligned} \quad (10)$$

Here, c_n represents the fact that the $q\bar{q}g$ and the $q\bar{q}g_n^*$ vertex factors differ by a $\sqrt{2}$ (*i.e.*, $c_0 = 1$, $c_{n>0} = 2$). In the amplitude-squared, it is therefore necessary to evaluate terms of the form

$$\frac{1}{2} \left[D_{\text{eff}}^*(\hat{v}) D_{\text{eff}}(\hat{w}) + D_{\text{eff}}(\hat{v}) D_{\text{eff}}^*(\hat{w}) \right] = \sum_{m,n=0}^{\infty} c_m c_n \frac{\hat{v}'_m \hat{w}'_n + m_m \Gamma_m m_n \Gamma_n}{(v_m^2 + m_m^2 \Gamma_m^2)(w_n^2 + m_n^2 \Gamma_n^2)}, \quad (11)$$

where \hat{v} and \hat{w} are any of the three usual (subprocess) Mandelstam variables (*i.e.*, $\hat{v}, \hat{w} \in \{\hat{s}, \hat{t}, \hat{u}\}$), and \hat{v}'_n represents the subtraction of m_n^2 from \hat{v} (*i.e.*, $\hat{v}'_n \equiv \hat{v}_n - m_n^2$). (In Eq. (11) we make an exception and include the $n = 0$ and $n > 0$ modes together for conciseness.) This sum converges somewhat rapidly.[†] Since $\sqrt{\hat{s}}$ runs up to 14 TeV for the LHC, the sum can be truncated after a couple dozen terms (*i.e.*,

*We neglect the contributions from cases where multiple jets are produced, but only two of them pass the various cuts.

[†]When generalizing to the case where the gluons may propagate into more than one large extra dimension, the sum in the effective propagator is formally divergent. However, this problem has been widely addressed in the literature [12], where various solutions have been proposed.

when n becomes at least a couple of times greater than $14 \text{ TeV}/\mu$, where μ is the compactification scale). We choose $n_{max} = 50$. From five-momentum conservation, there are no internal g^* 's for any tree-level dijet diagrams involving external gluons (*e.g.*, the KK excitations do not affect the process $q\bar{q} \rightarrow gg$). The diagrams to which the KK excitations do contribute are illustrated in Fig. 2.

The total dijet cross section $\sigma(pp \rightarrow 2 \text{ jets})$ is obtained from the individual subprocess cross sections $\hat{\sigma}(ab \rightarrow cd)$ and the parton distributions $f_{a/A}(x_A, Q)$ and $f_{b/B}(x_B, Q)$ by integrating over the momentum fractions x_A and x_B and summing over all possible subprocesses $ab \rightarrow cd$:

$$\sigma(pp \rightarrow 2 \text{ jets}) = \sum_{ab \rightarrow cd} \int_{4p_T^2/s}^1 d\tau \frac{d\mathcal{L}}{d\tau} \hat{\sigma}(ab \rightarrow cd). \quad (12)$$

Here, p_T is the transverse momentum and $d\mathcal{L}/d\tau$ is the parton luminosity:

$$\frac{d\mathcal{L}}{d\tau} = \int_{\tau}^1 \frac{dx_A}{x_A} f_{a/A}(x_A, Q) f_{b/B}(x_B, Q). \quad (13)$$

We evaluate the CTEQ distribution functions [13] for the parton luminosity at $Q = p_T$, and impose the following cuts: The transverse momentum p_T is constrained to lie above some minimum p_T^{min} , while the rapidity is restricted to satisfy $|y| \leq 2.5$. The total cross section can also be separated into the SM cross section and the g^* cross section, which is due to the contributions of Fig. 2: $\sigma = \sigma_{SM} + \sigma_{KK}$. Although σ_{KK} includes the interference terms between g 's and g^* 's, it usefully represents the amount by which the total cross section exceeds the SM background. The KK contributions, along with the SM background, are shown in Fig.'s 3–4 for compactification scales in the range $1 \text{ TeV} \leq \mu \leq 10 \text{ TeV}$ and for transverse momentum as high as $p_T^{min} \leq 4 \text{ TeV}$.

The KK effect is actually quite large: For sufficiently high p_T^{min} ($\sim 2 \text{ TeV}$), the effect of the virtual exchanges of the g^* 's actually exceeds the SM background for compactification scales below 7 TeV . The effect becomes even more pronounced for yet higher p_T^{min} , where the KK contribution becomes several factors larger than the SM cross section. The trend continues beyond the 4 TeV shown, but the cross section is too small beyond this point to observe more than a couple of events per year at the anticipated integrated luminosity of the LHC ($2 \times 10^5 \text{ pb}^{-1}$). Final quark states due to the decay of a very massive g^* have very high p_T , thereby enhancing the ratio $R \equiv \sigma_{KK}/\sigma_{SM}$ for high p_T^{min} , which is where the g^* contribution actually exceeds the SM contribution. When $p_T^{min} = k\mu/2$ for $k \in \{1, 2, \dots\}$, there is a slight disturbance in the cross section plots, which is expected since this corresponds to an on-shell g^* contribution. Naturally, the disturbance is only discernible for small values of k . These discernible regions are indicated on the plots by the corresponding values of k .

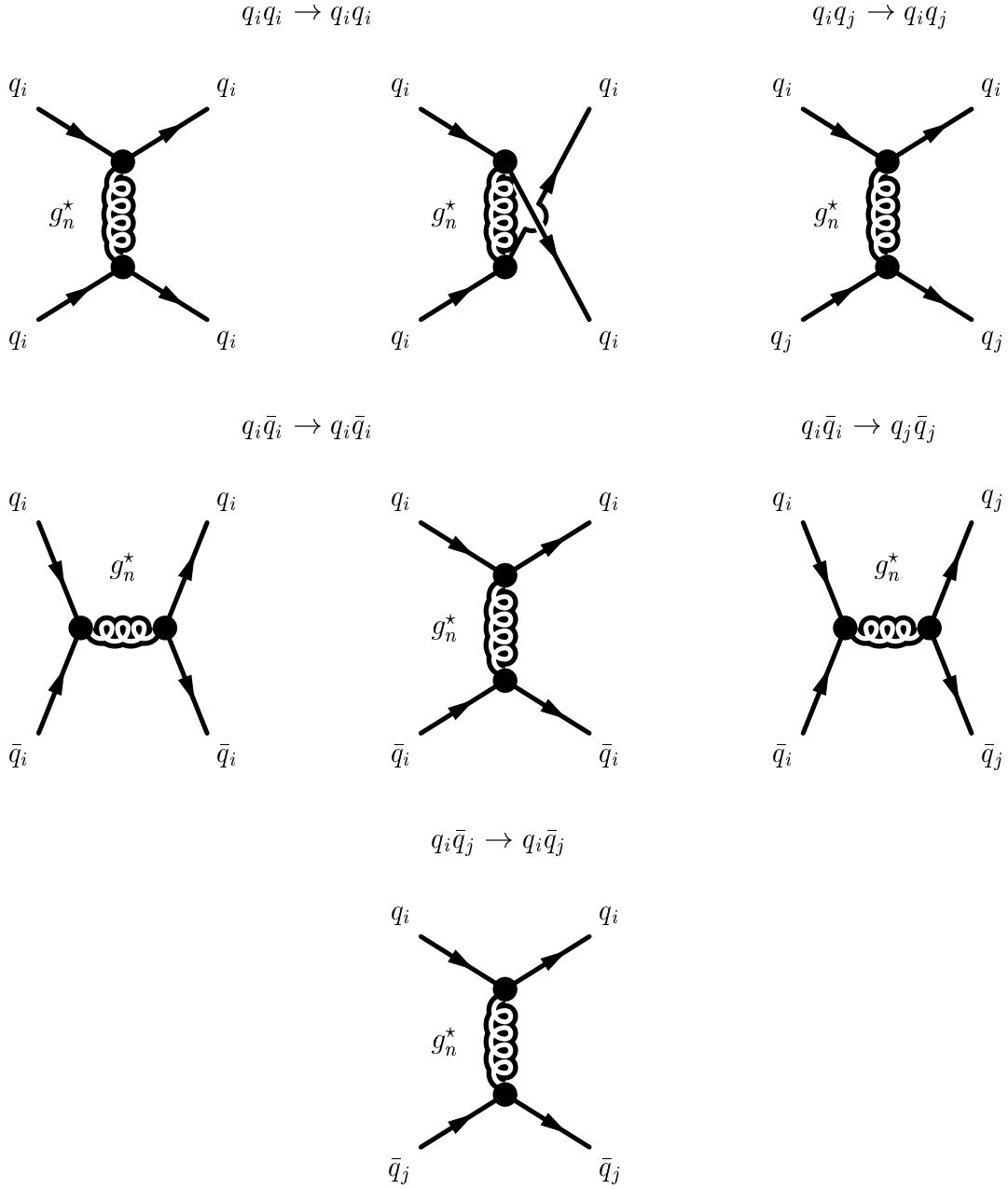


Figure 2: Dijet diagrams involving KK excitations of the gluons. The indices i and j represent distinct ($i \neq j$) quark flavors.

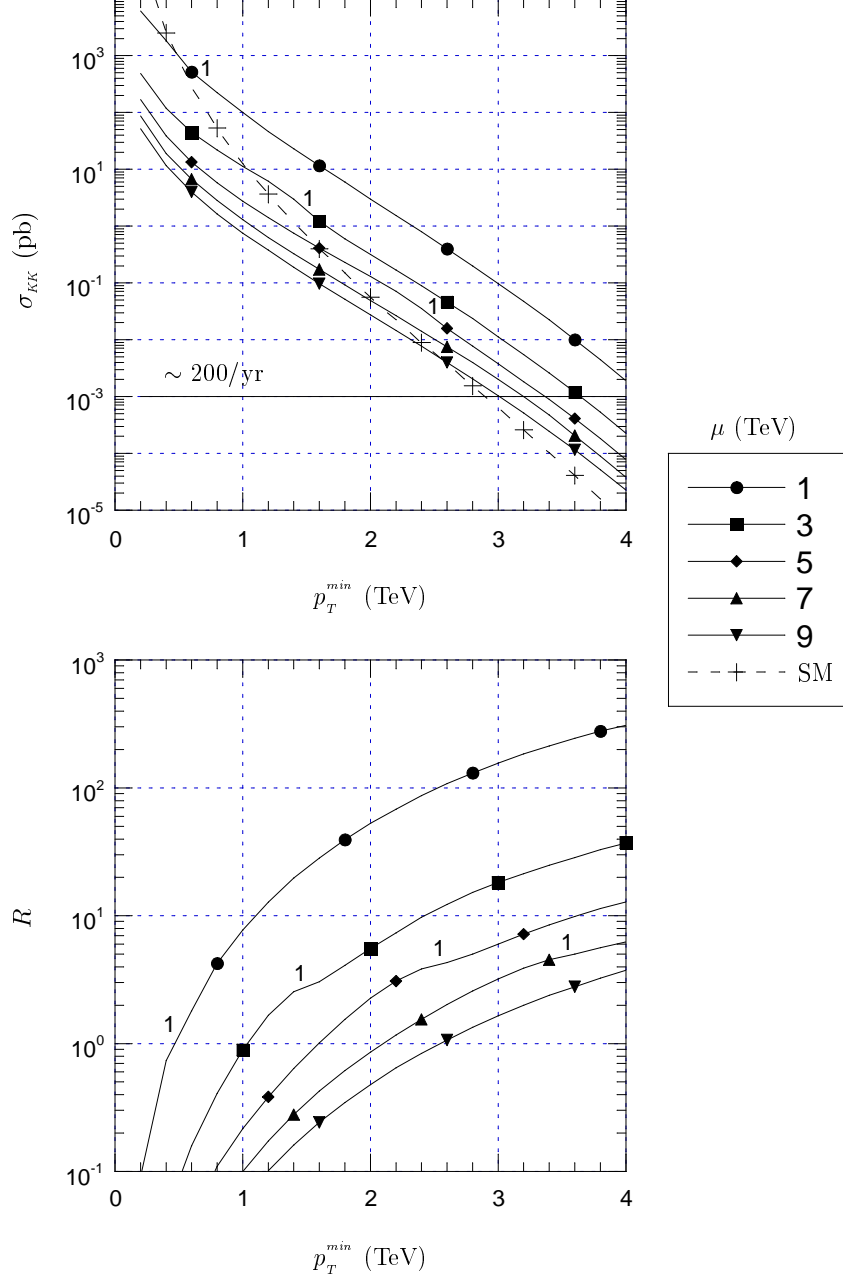


Figure 3: The contributions of the virtual exchanges of g^* 's to the LHC dijet production cross section, $\sigma_{KK} = \sigma - \sigma_{SM}$, (top) and the ratio of the KK contribution to the SM background, $R = \sigma_{KK}/\sigma_{SM}$, (bottom) are illustrated as a function of the minimum transverse momentum p_T^{min} for fixed values of the compactification scale μ . The solid horizontal line represents ~ 200 events/yr at the projected integrated luminosity. Discernible bumps in regions for which $p_T^{min} = k\mu/2$ are indicated by the corresponding value of $k \in \{1, 2, \dots\}$.

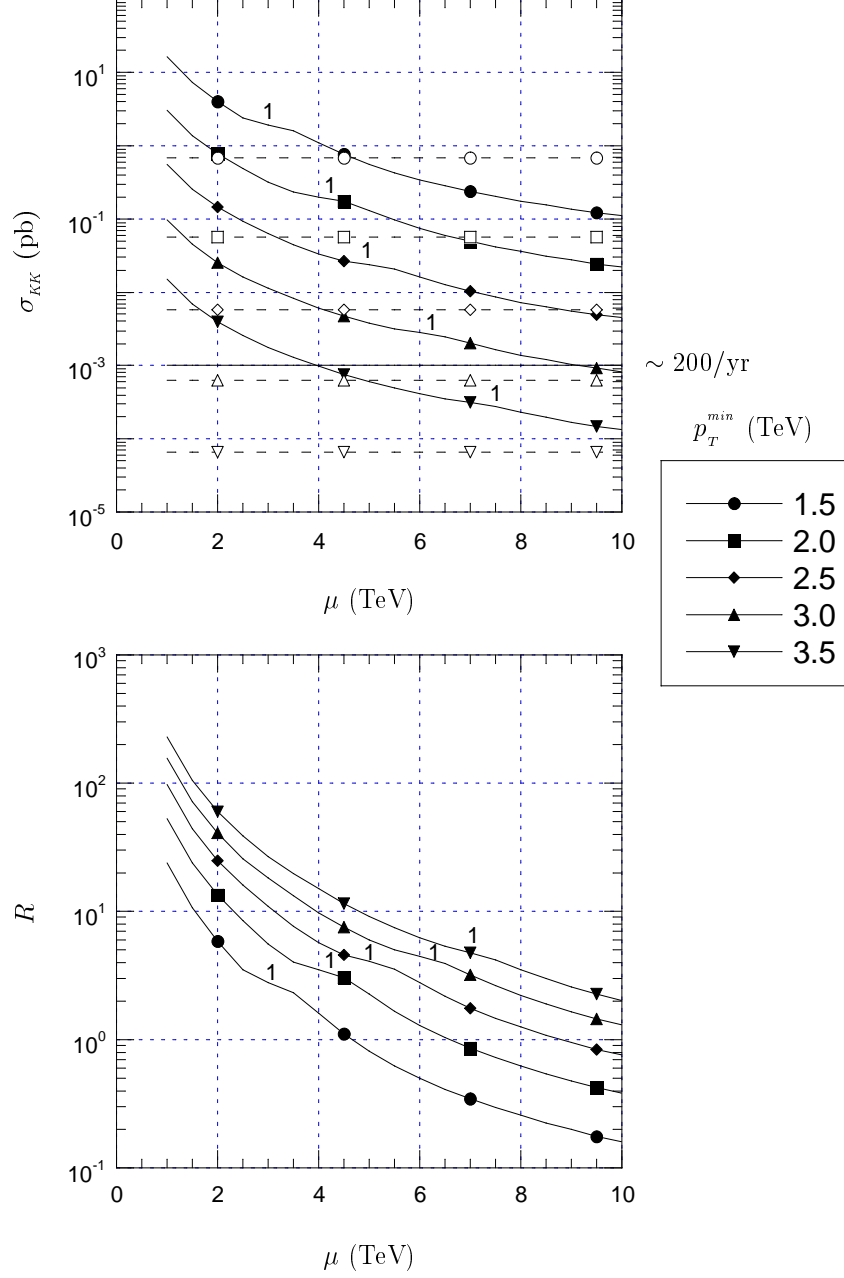


Figure 4: Same as Fig. 3, but as a function of the compactification scale μ for fixed values of the minimum transverse momentum p_T^{min} . The horizontal dashed lines represent the SM background.

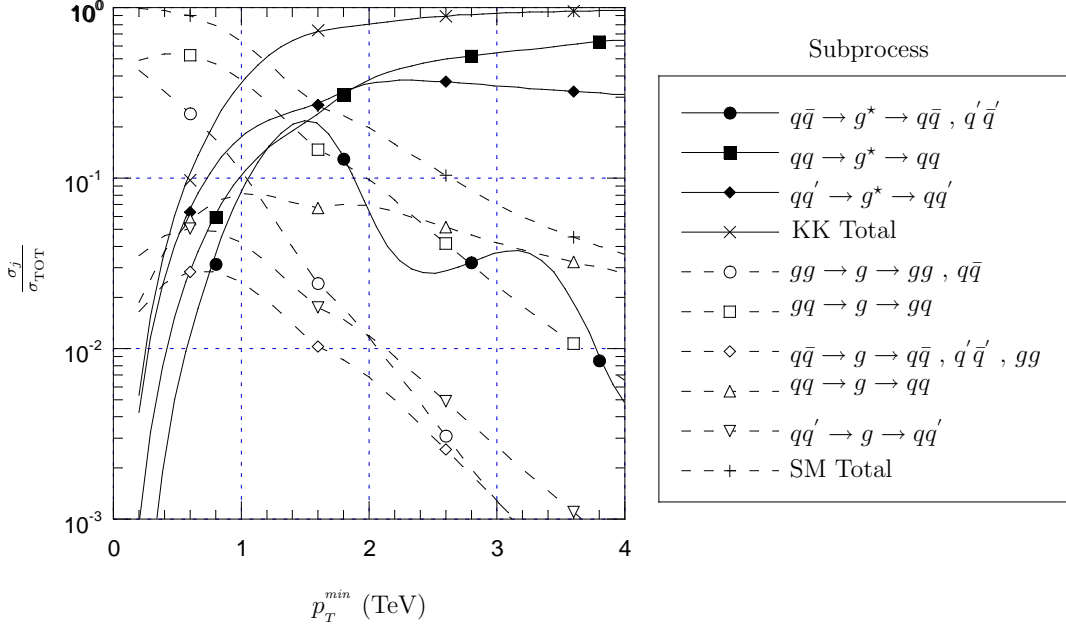


Figure 5: The partial contributions to the total dijet cross section are shown as a function of p_T^{min} , for $\mu = 3.5$ TeV.

The partial contributions of the various subprocesses to the full dijet KK (for a representative value of $\mu = 3.5$ TeV) and SM cross sections are illustrated in Fig. 5. At low p_T , the virtual g^* effect is greatest for subprocesses with two different initial quarks, while, at high p_T , it is largest for subprocesses with identical initial quarks.

Fig. 6 shows the dijet differential cross section $d\sigma/dm$ as a function of the invariant mass m of the final state $q\bar{q}$ pair: The peaks are subtle, and positioned well below the SM background. The signal in the two-jet invariant mass distribution is well below the SM background unless the invariant mass is very large ($m > 5$ TeV). However, at the LHC, the cross sections are not large enough for the signal to be observable in this range of m . There are two reasons why the dijet invariant mass distribution does not give a good signal. First, the widths of the g^* 's are large such that the peaks corresponding to $m = \mu$ are not sharp nor tall enough. Secondly, most of the cross section for a given invariant mass comes from pairs which have relatively low p_T for which the SM background is very large. The decay of the resonant KK gluon, g^* , gives rise to high p_T for each of the jet pairs. It is only when we consider the final states where each of the jets have high p_T that the KK contributions exceed the SM background. In the invariant mass distribution, such high p_T contributions constitute only a very small part of the cross sections observable at the LHC energy.

Depicted in Fig. 7 are the effects produced by variation of the somewhat arbitrary choice of $Q = p_T^{min}$ for the SM background. The relative uncertainty in the SM background can be quite high, say 40 %, due to the ambiguity in the choice of Q , and other factors such as the choice of parton distributions. However, since the signal and

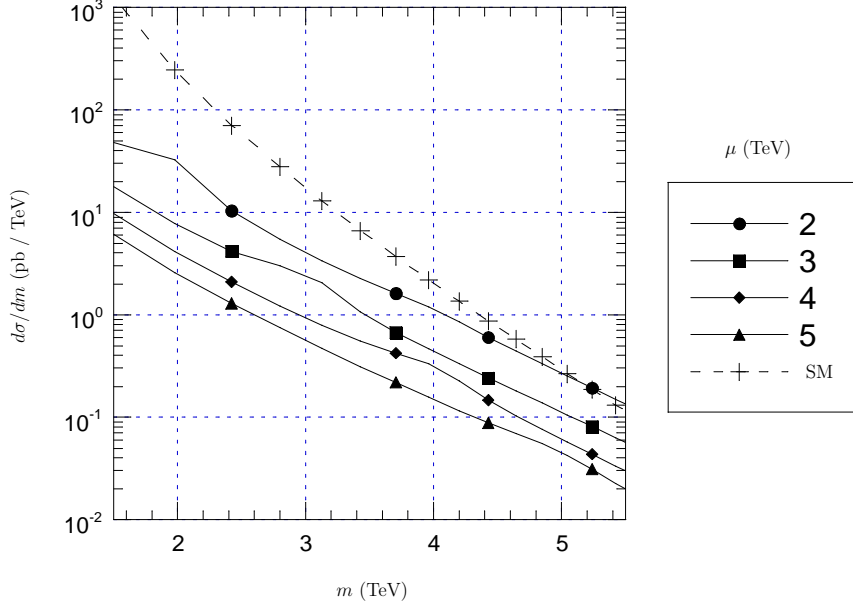


Figure 6: The differential cross section $d\sigma/dm$ is shown as a function of the invariant mass m of the $q\bar{q}$ pair. The peaks that are predicted to occur when the invariant mass m matches the compactification scale μ are subtle and located well below the SM signal.

the background are each calculated at tree-level, the uncertainties should somewhat cancel in the ratio, R . Thus, R provides a good measure of the relative KK effect. We point out that due to these uncertainties and the fact that one can not directly measure R , when working at tree-level it is necessary to look for signals that disagree with the SM by much more than 50%, probably as much as 100%, to be sure that we are indeed observing a signal for new physics. Therefore, the detection of KK excitations of the gluons is most favorable for regions of (p_T^{min}, μ) -space where the KK contribution is at least comparable to the SM background, and above the horizontal line (in Fig.'s 3–4) that marks an anticipated couple of hundred events per year.

For comparison, in Fig.'s 8–9 we also give the g^* cross section and its relation to the SM background for the Fermilab Tevatron $p\bar{p}$ collider running at $\sqrt{s} = 2$ TeV. The KK effect is much smaller than for the LHC because of the considerably more restrictive constraints on the transverse momentum. The g^* cross section is only comparable to the SM for compactification scales μ as high as about 2 TeV, and the relative uncertainty in the total dijet cross section must be quite precise in order to see a sizeable discrepancy for $\mu \sim 3$ TeV.

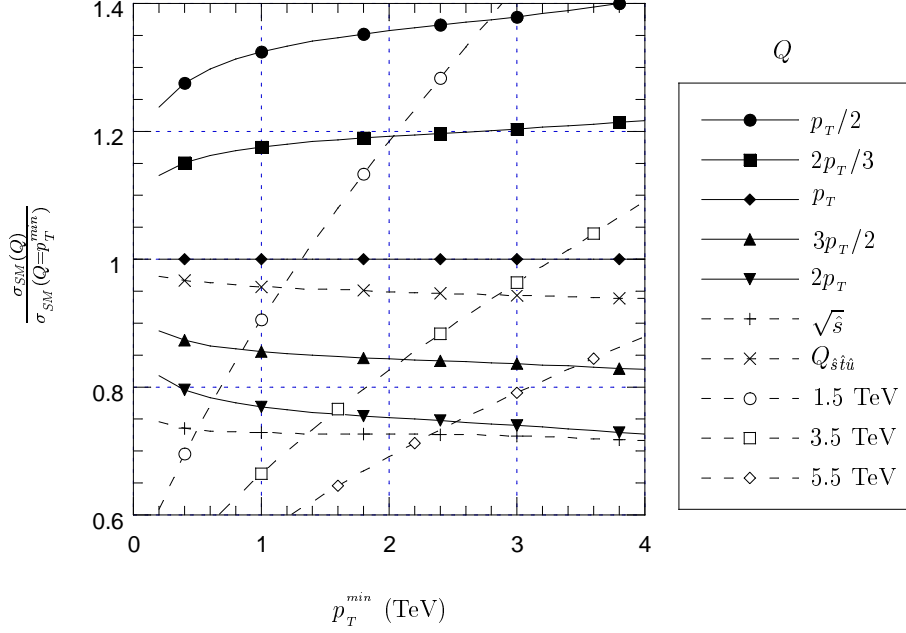


Figure 7: The effect that variation of the choice of Q has on the SM dijet background is shown as a function of the minimum transverse momentum, p_T^{min} . Here $Q_{\hat{s}\hat{t}\hat{u}} = \sqrt{\frac{\hat{s}\hat{t}\hat{u}}{\hat{s}^2 + \hat{t}^2 + \hat{u}^2}}$, and values in TeV (*e.g.*, 3.5 TeV) correspond to the choice of (constant) Q equal to a compactification scale at that particular scale.

4. Single On-Shell g^* Production

Three-jet KK final states predominantly* arise from subprocesses where a g^* is produced on-shell and subsequently decays into $q\bar{q}$, *e.g.*, via $q\bar{q} \rightarrow g_n^* \rightarrow g_n^* g \rightarrow q\bar{q}g$. We concentrate on the production of the g^* , postponing the consideration of its subsequent decay for the meantime. The subprocesses satisfying five-momentum conservation for which a g^* is produced on shell are:

$$\begin{aligned}
 q\bar{q} &\rightarrow g_n^* g \\
 qg &\rightarrow qg_n^* \\
 \bar{q}g &\rightarrow \bar{q}g_n^*,
 \end{aligned}
 \tag{14}$$

where the mode n of the external g^* is necessarily identical to that of any virtual g^* 's. Therefore, there is no summation over modes in these propagators; instead, the

The contributions of virtual g^ exchanges for which no external on-shell g^* 's are produced to the three-jet KK cross section contain an extra factor of $\alpha_s(Q)$ relative to the contribution of single on-shell g^* production. However, since virtual g^* exchange is significant for dijet production, the many virtual g^* exchange diagrams leading to three jets in the final state — for which no external g^* 's are produced on shell — may also have a significant effect. Although we do not calculate these purely virtual exchange contributions here, we do note that they would likely enhance our results.

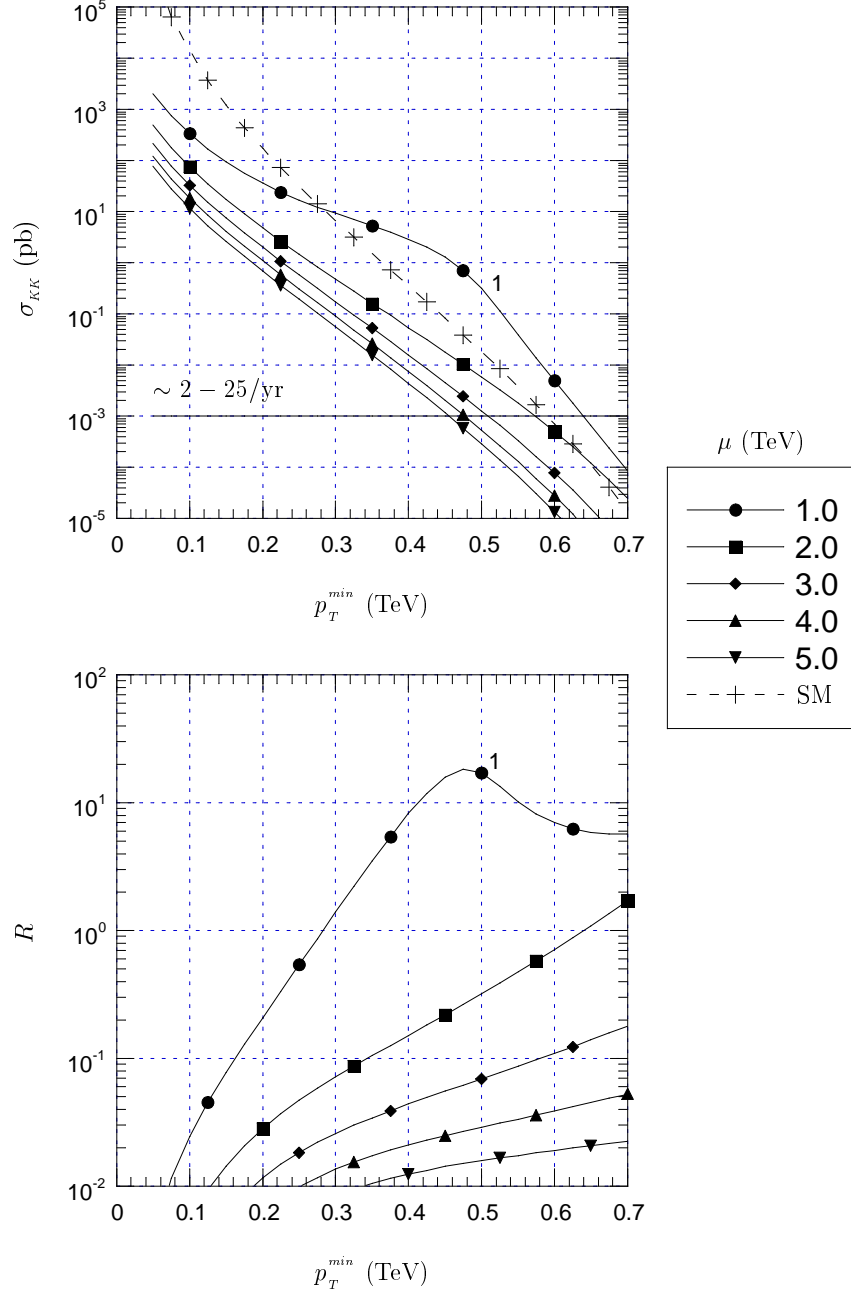


Figure 8: The contributions of the virtual exchanges of g^* 's to the Tevatron dijet production cross section, $\sigma_{KK} = \sigma - \sigma_{SM}$, (top) and the ratio of the KK contribution to the SM background, $R = \sigma_{KK}/\sigma_{SM}$, (bottom) are illustrated as a function of the minimum transverse momentum p_T^{\min} for fixed values of the compactification scale μ . The solid horizontal line represents ~ 2 (25) events/yr at the projected initial (final) Run 2 integrated luminosity. Discernible bumps in regions for which $p_T^{\min} = k\mu/2$ are indicated by the corresponding value of $k \in \{1, 2, \dots\}$.

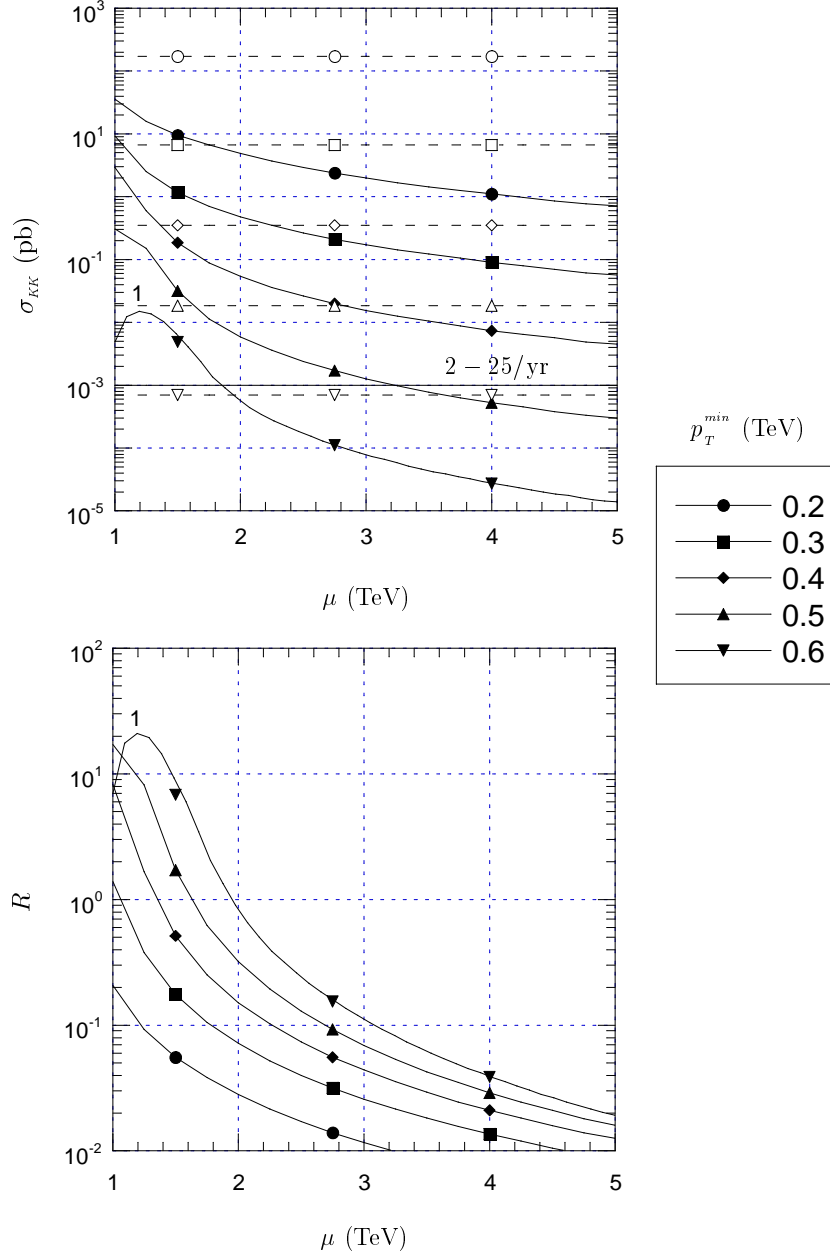


Figure 9: Same as Fig. 8, but as a function of the compactification scale μ for fixed values of the minimum transverse momentum p_T^{min} . The horizontal dashed lines represent the SM background.

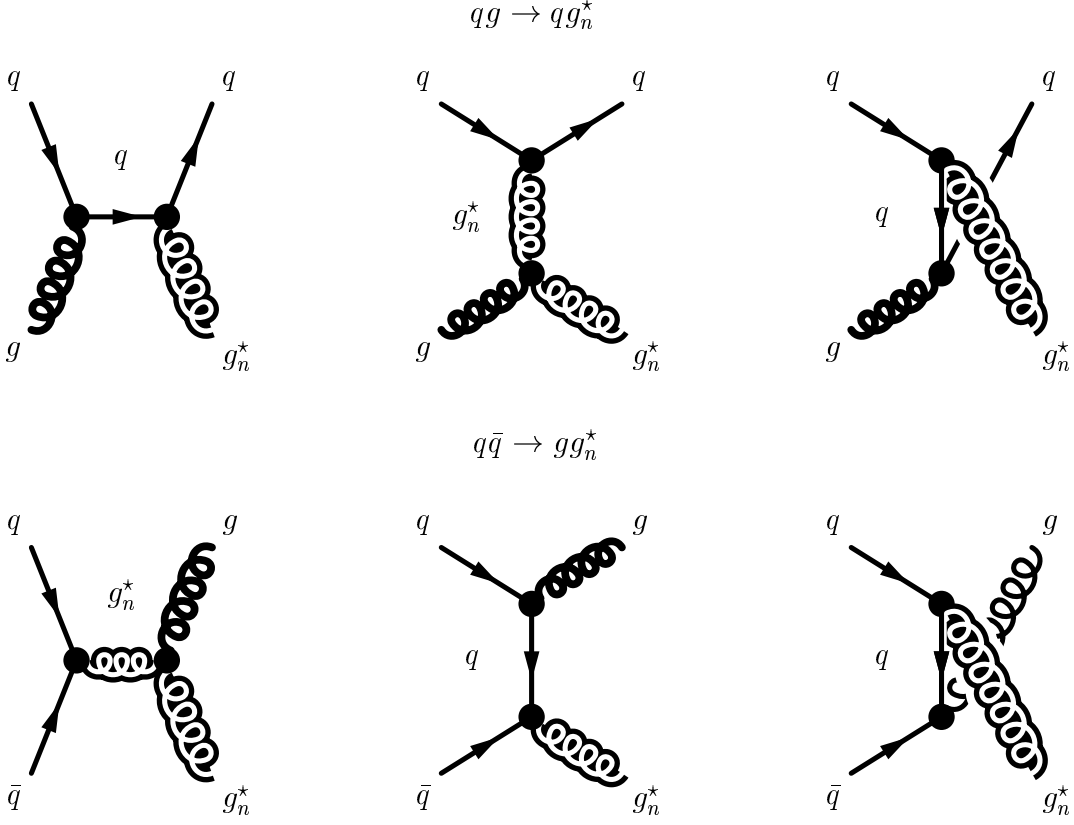


Figure 10: Diagrams involving the production of a single on-shell g^* . The diagrams for $\bar{q}g \rightarrow \bar{q}g_n^*$ are obtained by replacing q with \bar{q} in the diagrams for $qq \rightarrow qq_n^*$.

three-jet cross section involves a summation over the possible modes ($n \geq 1$) of the external g^* 's. The Feynman diagrams for these three KK subprocesses are illustrated in Fig. 10. The amplitude for $q\bar{q} \rightarrow g_n^*g$ is

$$\begin{aligned} \mathcal{M}(q\bar{q} \rightarrow g_n^*g) = & -i4\pi\alpha_s(Q)\bar{v}_j(p_1)\left[T_{ki}^e T_{jk}^f\left(\frac{V_{\rho\sigma}^t}{\hat{t}} + \frac{V_{\rho\sigma}^s}{\hat{s}'_n}\right)\right. \\ & \left.+ T_{ki}^f T_{jk}^e\left(\frac{V_{\rho\sigma}^u}{\hat{u}} - \frac{V_{\rho\sigma}^s}{\hat{s}'_n}\right)\right]u_i(p_2)\epsilon_e^{*\rho}(k_1)\epsilon_f^{*\sigma}(k_2), \end{aligned} \quad (15)$$

where the scale Q is identified with the mass of the g^* , \hat{v}'_n represents (as before) subtraction of m_n^2 from the Mandelstam variable $\hat{v} \in \{\hat{s}, \hat{t}, \hat{u}\}$ (*i.e.*, $\hat{v}'_n = \hat{v} - m_n^2$), and the $V_{\rho\sigma}^v$ tensors are given by

$$V_{\rho\sigma}^s = \sqrt{2}\gamma^\mu \left[(k_2 + 2k_1)_\sigma g_{\mu\rho} + (-k_1 + k_2)_\mu g_{\rho\sigma} - (2k_2 + k_1)_\rho g_{\sigma\mu} \right] \quad (16)$$

$$V_{\rho\sigma}^t = \sqrt{2}\gamma_\rho (\not{p}_1 - \not{k}_1)\gamma_\sigma \quad (17)$$

$$V_{\rho\sigma}^u = \sqrt{2}\gamma_\sigma (\not{k}_1 - \not{p}_2)\gamma_\rho. \quad (18)$$

After summing over final states and averaging over initial states, the resulting amplitude-squared is*

$$\bar{\Sigma} |\mathcal{M}(q\bar{q} \rightarrow g_n^* g)|^2 = \frac{8}{27} \pi^2 \alpha_s^2(Q) \left[\left(\frac{m_n^4}{\hat{s}'^2_n} + \frac{m_n^2}{\hat{s}'_n} \right) \left(8 \frac{\hat{s}'^2_n}{\hat{t}\hat{u}} - 18 \right) - 17 + 4 \frac{\hat{s}'^2_n}{\hat{t}\hat{u}} + 18 \frac{\hat{t}\hat{u}}{\hat{s}'^2_n} \right], \quad (19)$$

which is related to the amplitude-squared for $qg \rightarrow qg_n^*$ via crossing symmetry:

$$\bar{\Sigma} |\mathcal{M}(qg \rightarrow qg_n^*)|^2 = \frac{1}{9} \pi^2 \alpha_s^2(Q) \left[\left(\frac{m_n^4}{\hat{u}'^2_n} + \frac{m_n^2}{\hat{u}'_n} \right) \left(18 - 8 \frac{\hat{u}'^2_n}{\hat{s}\hat{t}} \right) + 17 - 4 \frac{\hat{u}'^2_n}{\hat{s}\hat{t}} + 18 \frac{\hat{s}\hat{t}}{\hat{u}'^2_n} \right]. \quad (20)$$

The amplitude-squared for $\bar{q}g \rightarrow \bar{q}g_n^*$ is in turn identical to that of $qg \rightarrow qg_n^*$ by time-reversal invariance. Upon integration over \hat{t} , the single g^* on-shell production cross sections assume the form

$$\sigma_{KK}(pp \rightarrow g^* + \text{jet}) = \frac{1}{2\pi} \sum_j \sum_{g_n^*} \int_{m_n^2/s}^1 dx_A \int_{m_n^2/s x_A}^1 dx_B f_{a/A}(x_A, Q) f_{b/B}(x_B, Q) \int_{-1}^1 dz \bar{\Sigma} |M_{jn}|^2 \frac{\hat{s}'_n}{\hat{s}^2}, \quad (21)$$

where the first summation runs over all possible subprocesses j producing a single g^* on-shell, and the second summation is over all g_n^* 's that can be produced for subprocess j in light of the given pp collider energy \sqrt{s} .[†] Observe that $M_{jn}(m_n) = M_{j1}(nm_1)$ so that $\sum_{n=1}^{n_{\max}} M_{jn}(m_n) = \sum_{n=1}^{n_{\max}} M_{j1}(nm_1)$. We are now prepared to account for the decay of the g_n^* into $q\bar{q}$ pairs. Working in the narrow width approximation, we integrate over the dimensionless solid angle $d\Omega_4/4\pi$ to obtain the total single on-shell g^* cross section (prior to cuts):

$$\sigma_{KK}(pp \rightarrow \text{jet} + g^* \rightarrow 3 \text{jets}) = \int \frac{d\Omega_4}{4\pi} \sigma_{KK}(pp \rightarrow g^* + \text{jet}). \quad (22)$$

*We employ *FORM* [14], a symbolic manipulation program, in the evaluation of the amplitudes-squared for single and double on-shell g^* production.

[†]Note that the scale $Q = m_n$ for the $n > 1$ modes exceeds the compactification scale μ . When $Q > \mu$, the running of $\alpha_s(Q)$ transforms from a logarithmic to a power law behavior [3]. This has the effect of reducing the contributions of the higher order modes to the total multijet cross sections [15], but only slightly at LHC energies since only a few KK modes can be produced on-shell.

The various cuts are performed by defining the two 4-momenta of the decaying particles in their center of mass frame in terms of Ω_4 (each decaying particle has momentum $m_n/2$) and boosting the two 4-momenta to the lab frame. In addition to the g^* cross section, we calculate the SM three-jet background following the outline of Ref. [16].

In addition to the cuts applied for dijet production, for three or four jets, we constrain final states to be separated by a cone of radius $R = \sqrt{(\Delta\phi)^2 + (\Delta\eta)^2} = 0.4$, where ϕ is the azimuthal angle and η is the pseudorapidity, which is related to the polar angle θ via $\eta = -\ln \tan(\theta/2)$. The single on-shell g^* production cross sections, along with the SM background, are plotted in Fig.'s 11–12 for $1 \text{ TeV} \leq \mu \leq 5 \text{ TeV}$ and $p_T^{min} \leq 2 \text{ TeV}$. High p_T cuts have a similar effect to that described for dijet production except that the $p_T^{min} = k\mu/2$ disturbances are much larger than the dijet case, which should be expected since the g^* is produced on-shell in the three-jet case considered here. Such discernible disturbances are indicated by the corresponding values of $k \in \{1, 2, \dots\}$. Again we terminate the p_T cuts when the number of anticipated events is quite scarce ($\sim 1/\text{yr}$). Although it is not as extreme as in the dijet case, the single on-shell g^* results also exceed the SM background for very high p_T^{min} . The partial contributions of the various subprocesses to the g^* (for a representative value of $\mu = 3.5 \text{ TeV}$) and SM cross sections are shown in Fig. 13. The $qg \rightarrow qg^*$ subprocess dominates over the range of interest, and $q\bar{q} \rightarrow gg^*$ only contributes to the KK dijet cross section significantly for low p_T . The effect of varying Q in the SM for three jets resembles the effect for two jets to a large degree (Fig. 14).

We point out that our calculation of the background for these three-jet final states is somewhat of an overestimate. In our signal, two of the jets come from the decay of an on-shell g^* . If we impose the condition that two of the jets cluster around the g^* mass for the SM background, the background to the signal ratio will be less. We did not impose that since we are not certain whether that will be possible to implement experimentally in the actual detection of the jets. If that is experimentally feasible, the background to our signal ratio will be less.

5. Double On-Shell g^* Production

Double on-shell g^* production is analogous to single on-shell g^* production, except that in this case the predominant KK subprocesses involve the production of two on-shell g^* 's which subsequently decay into $q\bar{q}$ pairs, *e.g.*, $q\bar{q} \rightarrow g \rightarrow g_n^* g_n^* \rightarrow q\bar{q} q\bar{q}$. Also, the single on-shell g^* case did not involve the $g_n^* g_m^* g_\ell^*$ nor the g - g - $g_n^* g_n^*$ vertices, which are now part of the picture. Focusing on the production of the g^* 's for the present and applying five-momentum conservation, the subprocesses for which two g^* 's are produced on shell are:

$$\begin{aligned} q\bar{q} &\rightarrow g_n^* g_n^* \\ q\bar{q} &\rightarrow g_n^* g_m^* \\ gg &\rightarrow g_n^* g_n^* , \end{aligned} \tag{23}$$

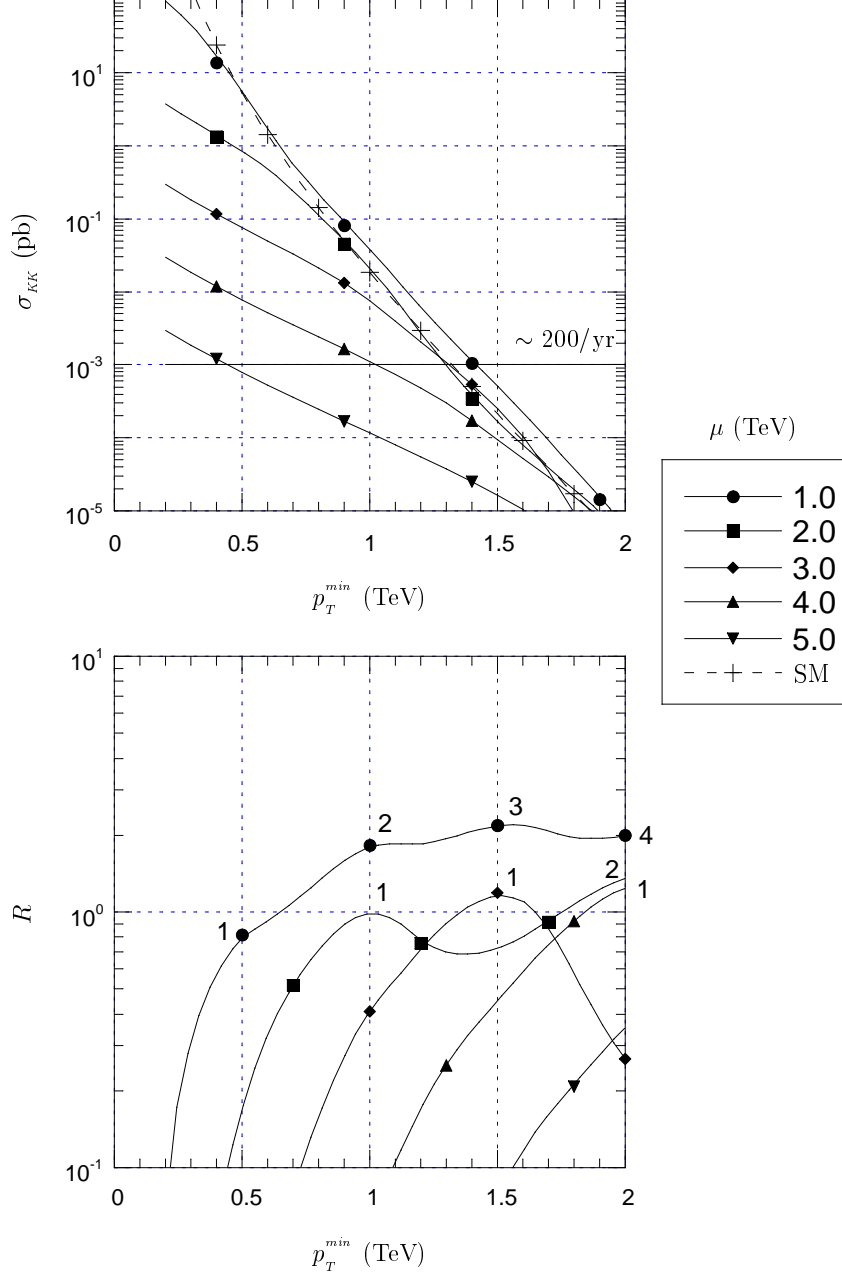


Figure 11: The contributions of the single-on shell production of g^* 's to the three-jet cross section at the LHC, $\sigma_{KK} = \sigma - \sigma_{SM}$, (top) and the ratio of the KK contribution to the SM background, $R = \sigma_{KK}/\sigma_{SM}$, (bottom) are illustrated as a function of the minimum transverse momentum p_T^{\min} for fixed values of the compactification scale μ . The solid horizontal line represents ~ 200 events/yr at the projected integrated luminosity. Discernible bumps in regions for which $p_T^{\min} = k\mu/2$ are indicated by the corresponding value of $k \in \{1, 2, \dots\}$.

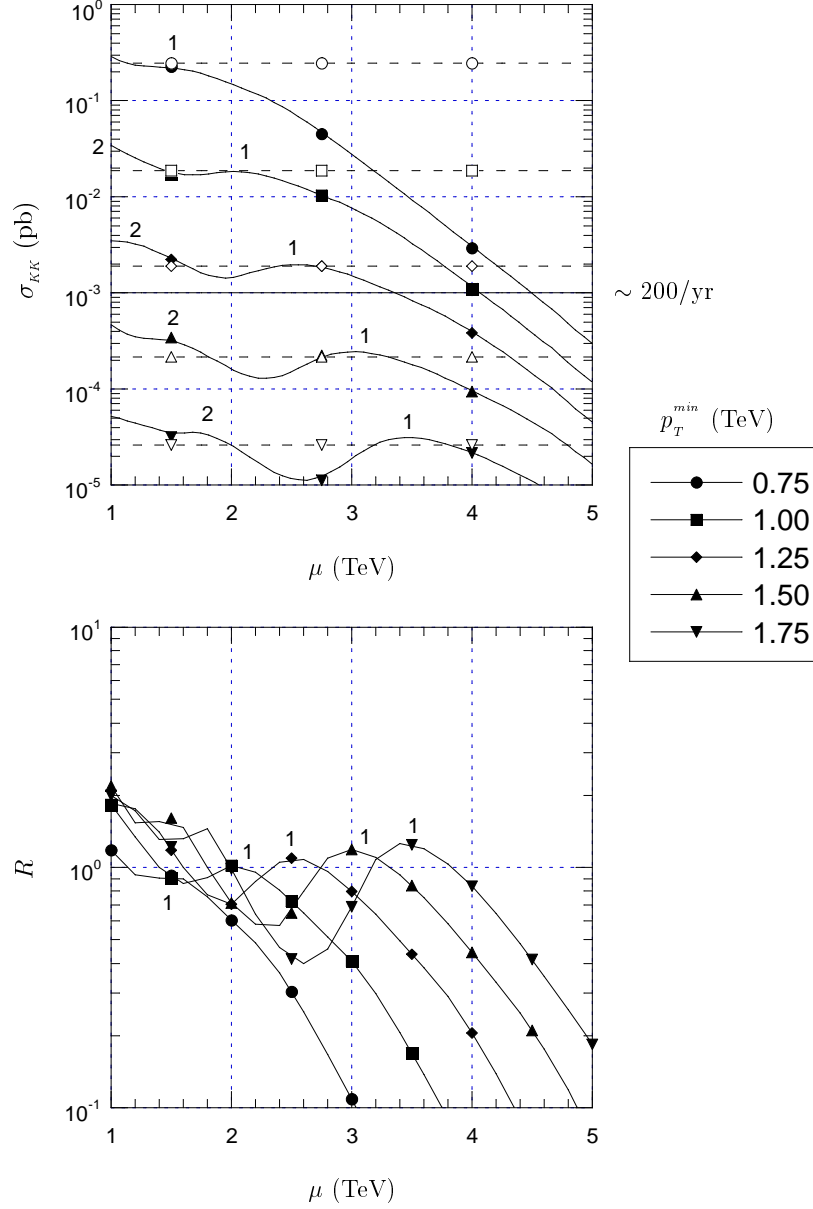


Figure 12: Same as Fig. 11, but as a function of the compactification scale μ for fixed values of the minimum transverse momentum p_T^{min} . The horizontal dashed lines represent the SM background.

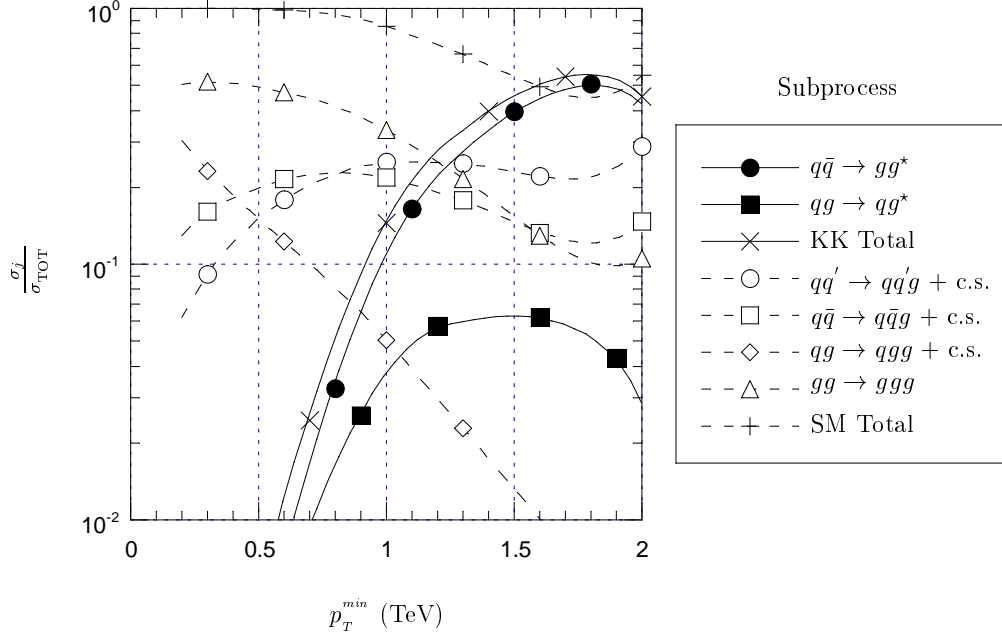


Figure 13: The partial contributions to the total three-jet cross section are shown as a function of p_T^{min} , for $\mu = 3.5$ TeV. Here, c.s. represents all subprocesses that are related by crossing symmetry.

where the two external g^* 's are necessarily in the same mode n for initial gluons, but not for initial quarks. The Feynman diagrams for these three KK subprocesses are illustrated in Fig. 15. The diagrams for $q\bar{q} \rightarrow g_n^* g_n^*$ are the same as for $q\bar{q} \rightarrow g_n^* g$ except that the \hat{s} -channel diagram can have either a virtual g or a virtual g_{2n}^* propagator. Thus, the amplitude for this process is the same as that given by Eq. (15) with the g_n^* propagator replaced by g and g_{2n}^* propagators, where the coefficient of the \hat{s} -channel amplitude is reduced by $1/\sqrt{2}$ for the g case. Likewise, the subprocess $q\bar{q} \rightarrow g_n^* g_m^*$ is simply $q\bar{q} \rightarrow g_n^* g_n^*$ with the s -channel altered for the possible propagators and the mass of either external line altered by a factor of m/n . The amplitude for $gg \rightarrow g_n^* g_n^*$ is

$$\begin{aligned} \mathcal{M}(gg \rightarrow g_n^* g_n^*) = & -i4\pi\alpha_s(Q) \left(f^{abc} f^{cef} \frac{V_{\alpha\beta\rho\sigma}^s}{\hat{s}} + f^{bec} f^{acf} \frac{V_{\alpha\beta\rho\sigma}^t}{\hat{t}_n'} \right. \\ & \left. + f^{bfc} f^{ace} \frac{V_{\alpha\beta\rho\sigma}^u}{\hat{u}_n'} + V_{\alpha\beta\rho\sigma}^{4abef} \right) \epsilon_a^\alpha(p_1) \epsilon_b^\beta(p_2) \epsilon_e^{*\rho}(k_1) \epsilon_f^{*\sigma}(k_2), \quad (24) \end{aligned}$$

where

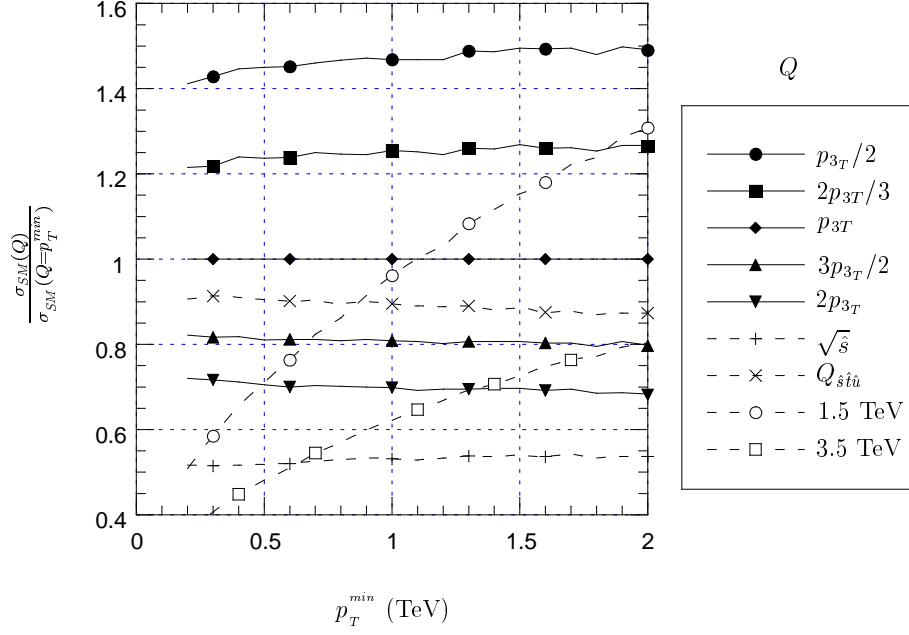


Figure 14: The effect that variation of the choice of Q has on the SM three-jet background is shown as a function of the minimum transverse momentum, p_T^{\min} . Here, p_{3T} is the transverse momentum of one of the jets, $Q_{\hat{s}\hat{t}\hat{u}} = \sqrt{\frac{\hat{s}\hat{t}\hat{u}}{\hat{s}^2 + \hat{t}^2 + \hat{u}^2}}$, and values in TeV (e.g., 3.5 TeV) correspond to the choice of (constant) Q equal to a compactification scale at that particular scale.

$$V_{\alpha\beta\rho\sigma}^s = \left[(-p_1 + p_2)_\mu g_{\alpha\beta} + (2p_1 + p_2)_\alpha g_{\beta\mu} - (p_1 + 2p_2)_\beta g_{\mu\alpha} \right] \cdot \left[(2k_1 + k_2)_\sigma g_{\nu\rho} + (-k_1 + k_2)_\nu g_{\rho\sigma} - (k_1 + 2k_2)_\rho g_{\sigma\nu} \right] g^{\mu\nu} \quad (25)$$

$$V_{\alpha\beta\rho\sigma}^t = \left[(p_1 + k_1)_\mu g_{\beta\rho} + (p_1 - 2k_1)_\beta g_{\rho\mu} + (-2p_1 + k_1)_\rho g_{\mu\beta} \right] \cdot \left[(2p_2 - k_2)_\sigma g_{\alpha\nu} + (-p_2 + 2k_2)_\alpha g_{\nu\sigma} - (p_2 + k_2)_\nu g_{\alpha\sigma} \right] g^{\mu\nu} \quad (26)$$

$$V_{\alpha\beta\rho\sigma}^u = \left[(p_1 + k_2)_\mu g_{\beta\sigma} + (p_1 - 2k_2)_\beta g_{\sigma\mu} + (-2p_1 + k_2)_\sigma g_{\mu\beta} \right] \cdot \left[(2p_2 - k_1)_\rho g_{\alpha\nu} + (-p_2 + 2k_1)_\alpha g_{\nu\rho} - (p_2 + k_1)_\nu g_{\alpha\rho} \right] g^{\mu\nu} \quad (27)$$

$$V_{\alpha\beta\rho\sigma}^{4abef} = f_{abc}f_{efc}(g_{\alpha\rho}g_{\beta\sigma} - g_{\alpha\sigma}g_{\beta\rho}) + f_{aec}f_{fbc}(g_{\alpha\sigma}g_{\beta\rho} - g_{\alpha\beta}g_{\sigma\rho}) + f_{afc}f_{bec}(g_{\alpha\beta}g_{\sigma\rho} - g_{\alpha\rho}g_{\beta\sigma}). \quad (28)$$

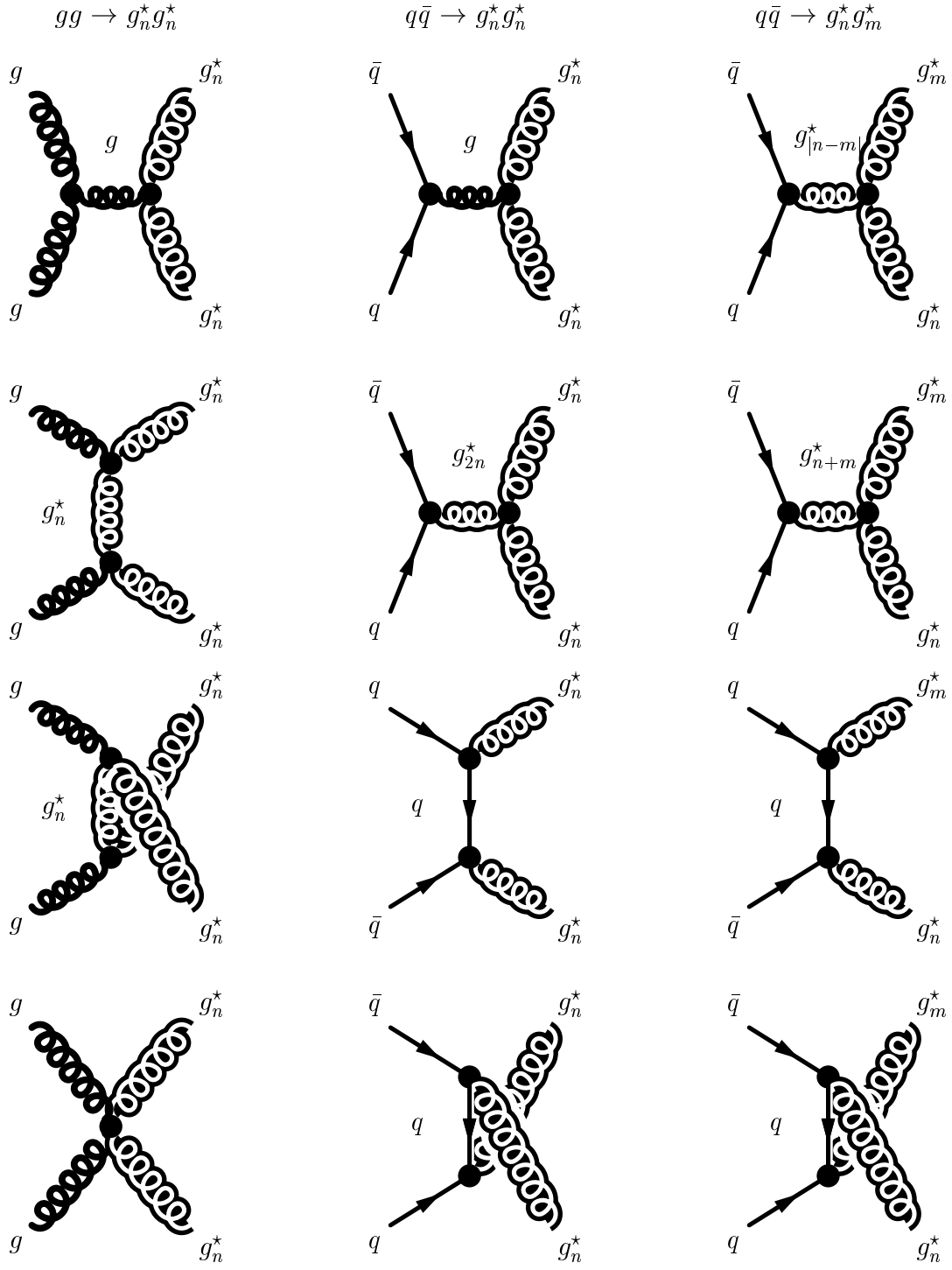


Figure 15: Diagrams involving the production of two on-shell g^* 's. The modes n and m are distinct ($n \neq m$).

The amplitudes-squared for these subprocesses, summed over final states and averaged over initial states, are obtained to be

$$\begin{aligned} \bar{\Sigma} |\mathcal{M}(q\bar{q} \rightarrow g_n^* g_n^*)|^2 = & \frac{8}{27} \pi^2 \alpha_S^2(Q) \left[648 m_n^6 \frac{1}{\tilde{s}_n \hat{t} \hat{u}} - 738 m_n^4 \left(\frac{1}{\tilde{s}_n \hat{s}} - 27 \frac{1}{\hat{s}^2} + 164 \frac{1}{\hat{t} \hat{u}} \right. \right. \\ & - 16 \frac{1}{\hat{t}^2} - 16 \frac{1}{\hat{u}^2} - 27 \frac{1}{\tilde{s}_n^2} \Big) \\ & + 9 m_n^2 \left(32 \frac{\hat{s}}{\hat{t} \hat{u}} - 144 \frac{1}{\hat{s}} \right) - 68 + 16 \frac{\hat{s}^2}{\hat{t} \hat{u}} + 18 \frac{\hat{t} \hat{u}}{\hat{s} \tilde{s}_n} \\ & \left. \left. + 27 \frac{\hat{t} \hat{u}}{\hat{s}^2} + 27 \frac{\hat{t} \hat{u}}{\tilde{s}_n^2} \right] \end{aligned} \quad (29)$$

$$\begin{aligned} \bar{\Sigma} |\mathcal{M}(q\bar{q} \rightarrow g_n^* g_m^*)|^2 = & \frac{8}{27} \pi^2 \alpha_S^2(Q) \left[-14 \frac{\hat{s} \hat{t}^2}{\hat{u}} + 2 \frac{\hat{t}^3}{\hat{u}} - 20 \hat{t} \hat{u} \right. \\ & + \left(-8 \frac{\hat{t}^2}{\hat{u}^2} m_m^2 m_n^2 + 30 \hat{t} m_m^2 + 14 \frac{\hat{t}}{\hat{u}} m_m^4 - 25 \frac{\hat{t}}{\hat{u}} m_m^2 m_n^2 \right. \\ & - 44 m_m^4 - 24 m_m^2 m_n^2 - 16 \frac{m_m^4 m_n^2}{\hat{u}} \\ & + 32 \frac{m_m^4 m_n^4}{\hat{u}^2} + 8 \frac{m_m^6 m_n^2}{\hat{t} \hat{u}} + 8 \frac{m_m^4 m_n^4}{\hat{t} \hat{u}} \\ & \left. \left. + m \leftrightarrow n \right) + t \leftrightarrow u \right] \frac{1}{\hat{s} - (m_m + m_n)^2} \frac{1}{\hat{s} - (m_m - m_n)^2} \end{aligned} \quad (30)$$

$$\begin{aligned} \bar{\Sigma} |\mathcal{M}(gg \rightarrow g_n^* g_n^*)|^2 = & \frac{9}{4} \pi^2 \alpha_S^2(Q) \left(\frac{s^2}{\hat{t}'_n \hat{u}'_n} - 1 \right) \\ & \cdot \left(6 \frac{m_n^4}{\hat{t}'_n \hat{u}'_n} - 6 \frac{m_n^2}{\hat{s}} + 2 \frac{\hat{s}^2}{\hat{t}'_n \hat{u}'_n} + \frac{\hat{t}'_n \hat{u}'_n}{\hat{s}^2} - 4 \right), \end{aligned} \quad (31)$$

where $\tilde{s}_n \equiv \hat{s} - 4m_n^2$. (In our notation, the replacements indicated by $t \leftrightarrow u$ do not affect the two terms that involve neither t nor u .)

We point out that in our results for the matrix element squares, as given in Eqs. (29 – 31), there are no terms that grow with energy, and the matrix elements for these subprocesses are tree-unitary. This is not true for the individual diagrams for the subprocesses: There are delicate cancellations between the diagrams for each subprocess. These cancellations occur only because of the relations among the couplings as dictated by the compactification of the five-dimensional KK theory to four dimensions, and also due to the special relations for the masses of the various KK states. For example, in the process $q\bar{q} \rightarrow g_n^* g_n^*$, the presence of the g_{2n}^* exchange is crucial with its mass $2n\mu$ and its coupling as dictated by the KK Yang-Mills theory. This is a new example of tree-unitarity for a class of massive vector boson theories other than the known spontaneously broken gauge theories [17].

These subprocess j amplitudes-squared combine to give the total KK cross section for g_n^* 's produced on-shell as

$$\sigma_{KK}(pp \rightarrow g^*g^*) = \frac{1}{4\pi} \sum_j \sum_{g^*\text{pairs}} \int_{\rho_{mn}}^1 dx_A \int_{\rho_{mn}/x_A}^1 dx_B f_{a/A}(x_A, Q) f_{b/B}(x_B, Q) \int_{-1}^1 dz \bar{\Sigma} |M_j|^2 \frac{1}{\hat{s}} \sqrt{1 - \frac{(m_m + m_n)^2}{\hat{s}}}, \quad (32)$$

where $\rho_{mn} = (m_m + m_n)^2/s$ and the second summation runs over all g_n^*, g_m^* pairs that can be produced for energy \sqrt{s} . Again, we apply the narrow width approximation to account for the decay of the g^* 's into $q\bar{q}$ pairs:

$$\sigma_{KK}(pp \rightarrow g^*g^* \rightarrow 4\text{jets}) = \int \frac{d\Omega_5}{4\pi} \int \frac{d\Omega_7}{4\pi} \sigma_{KK}(pp \rightarrow g^*g^*). \quad (33)$$

We employ the same cuts utilized for the single g^* case. Illustrated in Fig. 16 are the four-jet KK cross sections for $1.0 \text{ TeV} \leq \mu \leq 3.5 \text{ TeV}$, and $p_T^{\min} \leq 1.5 \text{ TeV}$. High p_T cuts have a similar effect to that described for single g^* production. The KK cross section is considerably smaller for double g^* production as compared to the single g^* case, which itself is much smaller than the dijet case: For double g^* production, the KK cross section is too small to expect more than a couple of events per year for a compactification scale in excess of 3.5 TeV, regardless of the SM four-jet background. The subprocess with initial quarks is about a factor of 6 larger than the contribution from initial gluons, which can be explained by the fact that it is partially magnified by the factors of $\sqrt{2}$ in the $q\bar{q}g^*$ vertices. Also, the production of two g^* 's with different modes is negligible compared to the case when they have identical modes because there can not be a gluon propagator in the s-channel in the former case.

6. Conclusions

In this work, we have investigated the phenomenology of a class of string-inspired models in which the SM gauge bosons can propagate into one TeV-scale extra dimension. Specifically, we calculate the effects that the KK excitations of the gluons have on multijet final states at very high energy hadronic colliders such as the LHC or upgraded Tevatron Run 2.

At the LHC ($\sqrt{s} = 14 \text{ TeV}$), we found a large enhancement, relative to the SM, of the dijet cross sections at high p_T , while at the upgraded Tevatron we found an effect that is considerably smaller. The effect is observable at the LHC for a compactification scale $\mu \lesssim 7 \text{ TeV}$, for a wide range of very high p_T . For example, with a minimum p_T for each of the jets of 2 TeV, the dijet cross section is about three times larger than that of the SM for $\mu = 5 \text{ TeV}$. Thus, the measurements of the dijet cross sections at

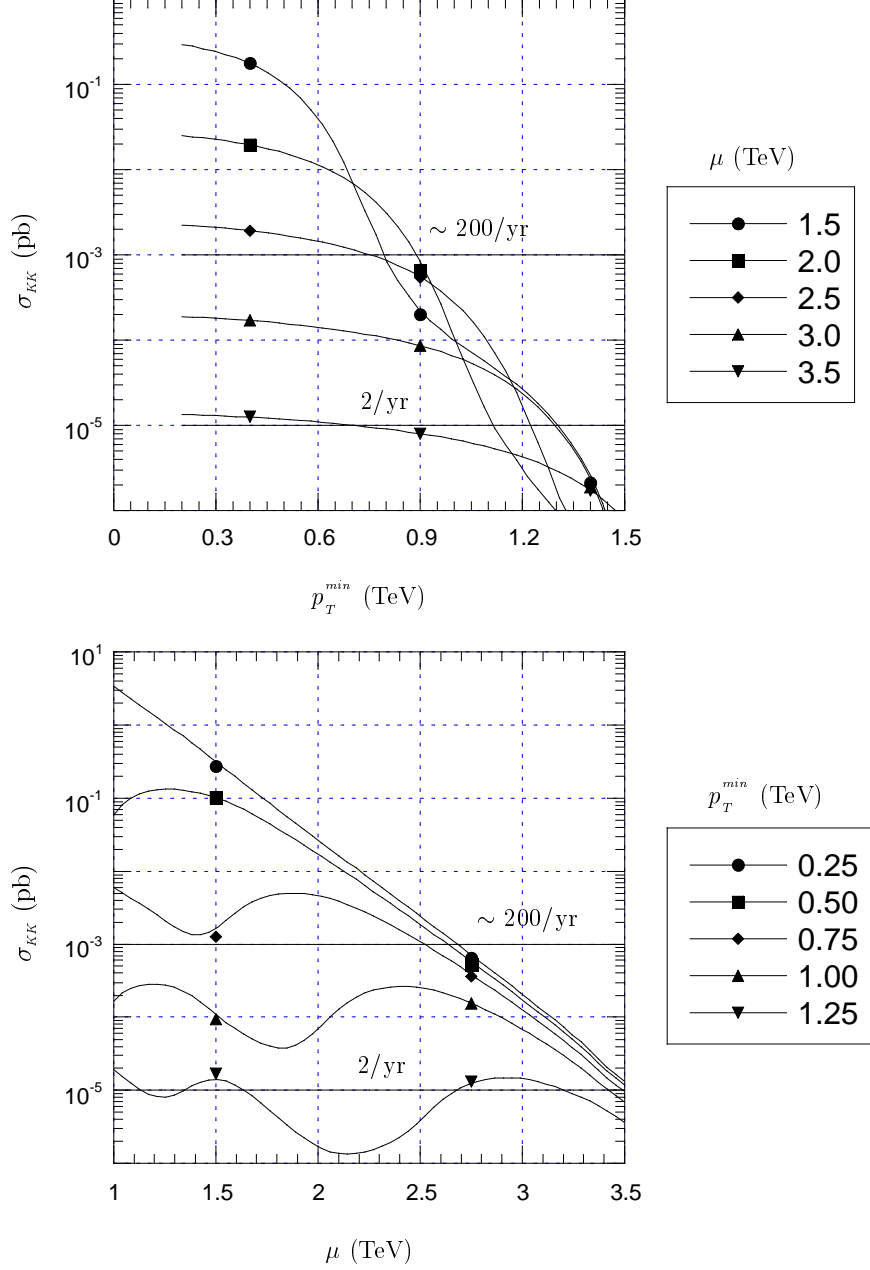


Figure 16: The contributions of the double-on shell production of g^* 's to the four-jet cross section at the LHC, $\sigma_{KK} = \sigma - \sigma_{SM}$, are illustrated as a function of the minimum transverse momentum p_T^{min} for fixed values of the compactification scale μ (top) and as a function of μ for fixed p_T^{min} (bottom).

the LHC will either discover the indirect effects of the KK modes of the gluons or set a bound on μ of about 7 TeV, which is significantly higher than the current bound of about 2 TeV. The effect is much less discernible at the upgraded Tevatron, and will not be observed for $\mu \gtrsim 2$ TeV. For three jets in the final state, in which two of the jets are the decay products of an on-shell g^* , at high p_T at the LHC, the KK enhancement over the SM cross sections is much smaller than for the dijet case. For example, with a minimum p_T of each of the jets of 1.5 TeV, the cross section is enhanced only by about 100% for $\mu = 3$ TeV. Although the dijet effect is much greater, three-jet final state measurements can offer additional confirming information if a large effect is seen in dijet final state measurements. For four jets in the final state from double on-shell g^* production, again the cross sections are rather small unless $\mu \lesssim 2.5$ TeV.

In the case of single or double on-shell g^* production leading to three or four jets, respectively, in the final state, the on-shell g^* 's subsequently decay primarily (the exceptions involve loop corrections) to quark and anti-quark pairs. These quark and anti-quark decay products will have very high p_T because the mass of the g^* is quite high (some multiple of the compactification scale, which is at least a TeV). If the invariant mass of the parent particle can be reconstructed using the measured high p_T of the jets, then that will be the clear signal of the first KK excitation of the gluons. In the three-jet case, such reconstruction must be done for each pair-wise configuration. Thus, for three jets in the final state, although the total cross section is not much larger than the SM background, such an invariant mass peak could potentially stand well above the SM background.

Now, we discuss some of the uncertainties in our calculations and results. Firstly, in the parton distribution function $f_{a/A}(x_A, Q)$ and the strong coupling $\alpha_s(Q)$, our results are somewhat sensitive to the choice of the scale Q . We chose $Q = p_T$ for the SM background as well as for the KK contribution to the dijet signal, and $Q = m_n$ (*i.e.*, the mass of the g^*) for single and double g^* production. We varied Q from $p_T/2$ to $2p_T$ for two or three jets in the final state for the SM background, and found an enhancement of about 40% for $p_T/2$ and a reduction of about 30% for $2p_T$ compared to $Q = p_T$. Thus, if the KK effect does not exceed the SM background significantly, it may be difficult to discern in light of the uncertainty arising from the choice of Q . However, for two jets only, we employ the same value for Q in the KK and SM cases, such that this uncertainty has less relative effect on the ratio R . Therefore, R can be somewhat smaller for two jets than three or more jets and still provide indirect evidence of KK excitations of the gluons. Secondly, in the calculations of three- and four-jet cross sections, we have only considered the production of g^* 's on-shell and their subsequent decays. We have not included those diagrams involving virtual g^* 's. Such virtual g^* contributions will naturally be small because they are higher order in the strong coupling constant $\alpha_s(Q)$. However, there are many virtual g^* diagrams (especially for four-jet diagrams) which may lead to a sizeable total contribution. Inclusion of these virtual g^* diagrams would enhance our three- and four-jet signals, thereby producing a somewhat greater effect. Finally, we have evaluated the running

of the strong coupling constant $\alpha_s(Q)$ with the usual logarithmic behavior of the SM. This is fine for $Q \leq \mu$, but when $Q > \mu$, the decrease is a power law behavior, in which case $\alpha_s(Q)$ would be somewhat smaller. However, since in most of our calculations, the scale Q (which is equal to p_T in the dijet case and m_n otherwise) is less than μ or does not exceed μ by much, the net effect would be only a relatively small reduction of our calculated cross sections (in our scenario with only one extra dimension).

Finally, we address the issue of how to distinguish the signal due to KK excitations from other new physics that might produce a similar collider signal. For example, the colorons [18] in the top color model produce effects similar to those of the KK excitations of the gluons. The eight colorons are like eight heavy gluons with the same mass, whereas, in the KK case, there is an infinite tower of increasing masses, $m_n = n\mu$ ($n = 1, 2, \dots$). One important distinguishing feature between the two cases is the difference in the details of the decay modes of the colorons and the KK excitations of the gluons. While the branching ratios of the KK g^* 's to the various quark flavors are identical, the branching ratios of the coloron to various flavors of quarks ($q_i \bar{q}_i$, $i \in \{u, d, c, s, t, b\}$) depends on the mixing angle between the two SU(3)'s, SU(3)_I and SU(3)_{II}. In the limit of zero mixing angle, the colorons couple only to $t\bar{t}$ and $b\bar{b}$. Thus, while the KK g^* 's decay equally to various quark flavors, the coloron decay is flavor-dependent. In the small mixing case, the dominant decays will be to $t\bar{t}$ and $b\bar{b}$. For the $t\bar{t}$ decay, the p_T of the jets coming from the subsequent decay of the top quark will be reduced. Thus, the dijet signal at very high p_T would be much stronger in the KK case than in the coloron case.

We are grateful to K.S. Babu, J.D. Lykken, and J.D. Wells for useful discussions. The work of DD was supported in part by the U.S. Department of Energy Grant Number DE-FG03-93ER40757; the work of CM and SN by DE-FG03-98ER41076.

Appendix

The generalization of the 4D SM Lagrangian density to the 5D Lagrangian density leads to 5D gluon field strength tensors $F_{MN}^a = \partial_M A_N^a - \partial_N A_M^a - g_5 f^{abc} A_M^b A_N^c$ described by

$$\begin{aligned} \mathcal{L}_5 &= -\frac{1}{4} F_{MN}^a F^{MNa} + i\bar{q}\gamma^\mu D_\mu q \delta(y) \\ &= -\frac{1}{4} \left(F_{\mu\nu}^a F^{\mu\nu a} + 2F_{\mu 4}^a F^{\mu 4a} \right) \\ &\quad + i\bar{q}\gamma^\mu D_\mu q \delta(y), \end{aligned} \tag{34}$$

where g_5 is the 5D strong coupling, A_M^a is the 5D gluon field, a, b, c are the usual gluon color indices, D_μ is the usual 4D covariant derivative, μ, ν are the usual 4D space-time indices, $M, N \in \{0, 1, \dots, 4\}$ are 5D space-time indices, and $\delta(y)$ represents that the SM fermions are localized in the D₃ brane with $y = 0$. The terms representing the

kinetic energy and interactions between the g and g^\star fields arise from the contraction of the $F_{\mu\nu}^a$'s:

$$\begin{aligned}
F_{\mu\nu}^a F^{\mu\nu a} &= \partial_\mu A_\nu^a \partial^\mu A^{\nu a} - \partial_\nu A_\mu^a \partial^\mu A^{\nu a} \\
&\quad - \partial_\mu A_\nu^a \partial^\nu A^{\mu a} + \partial_\nu A_\mu^a \partial^\nu A^{\mu a} \\
&\quad - 2g_5 f^{abc} A_\mu^b A_\nu^c \left(\partial^\mu A^{\nu a} - \partial^\nu A^{\mu a} \right) \\
&\quad - g_5^2 f^{abc} f^{ade} A_\mu^b A_\nu^c A^{\mu d} A^{\nu e}.
\end{aligned} \tag{35}$$

Similarly, the mass terms for the g_n^\star 's stem from the contraction of the $F_{\mu 4}^a$'s:

$$F_{\mu 4}^a F^{\mu 4 a} = \partial_4 A_\mu^a \partial^4 A^{\mu a}, \tag{36}$$

where the gauge choice $A_4^a = 0$ has been imposed. The remaining interaction of the g^\star 's involves the quark fields and is governed by the term in Eq. (34) involving the covariant derivative. We consider compactification on a S^1/Z_2 orbifold and make the identification $y \rightarrow -y$ such that $A_\mu^a(x, -y) = A_\mu^a(x, y)$. The fields $A_\mu^a(x, y)$ can then be Fourier expanded in terms of the compactified dimension $y = r\phi$ as

$$A_\mu^a(x, y) = \frac{1}{\sqrt{\pi r}} \left[A_{\mu 0}^a(x) + \sum_{n=1}^{\infty} A_{\mu n}^a(x) \cos(n\phi) \right], \tag{37}$$

where the normalization of $A_0^a(x)$ for the gluon field is one-half that of $A_n^a(x)$ for the KK excitations.

Integration over the compactified dimension y then gives the effective 4D theory. The terms from the integration of $-\frac{1}{4}F_{\mu\nu}^a F^{\mu\nu a}$ over y that are quadratic in the fields $A_\mu^a(x, y)$ give rise to kinetic energy terms in the effective 4D Lagrangian density of the form

$$\begin{aligned}
-\frac{1}{4} \int_0^{\pi r} \partial_\mu A_\nu^a(x, y) \partial^\mu A^{\nu a}(x, y) dy &= -\frac{1}{4} \left[\partial_\mu A_{\nu 0}^a(x) \partial^\mu A_0^{\nu a}(x) \right. \\
&\quad \left. + \frac{1}{2} \sum_{n=1}^{\infty} \partial_\mu A_{\nu n}^a(x) \partial^\mu A_n^{\nu a}(x) \right].
\end{aligned} \tag{38}$$

It is then necessary to rescale the fields as

$$A_{\mu 0}^a(x) \rightarrow A'_{\mu 0}{}^a(x), A_{\mu n}^a(x) \rightarrow A'_{\mu n}{}^a(x) \equiv \frac{A_{\mu n}^a(x)}{\sqrt{2}} \tag{39}$$

in order to canonically normalize the kinetic energy terms. Therefore, the mass and interaction terms must be expressed in terms of the rescaled fields, $A'_{\mu 0}(x)$ and $A'_{\mu n}(x)$. The masses of the KK excitations of the gluons arise from the integration of $F_{\mu 4}^a F^{\mu 4 a}$ over y :

$$-\frac{1}{4} \int_0^{\pi r} \partial_4 A_\mu^a(x, y) \partial^4 A^{\mu a}(x, y) dy = -\frac{1}{2} \frac{n^2}{r^2} \sum_{n=1}^{\infty} A'_{\mu n}(x) A'^{\mu a}_n(x). \quad (40)$$

The mass of the g_n^* is then identified as $m_n = n\mu$, where μ is the compactification scale ($\mu = 1/r$).

The Feynman rules for vertices involving g^* 's follow from the interaction terms. The interactions of the g^* 's with the quark fields originate from the term in the 5D Lagrangian density involving the covariant derivative. The delta function, which constrains the quark fields to the wall, takes care of the integration. Thus, the $q\bar{q}g^*$ vertex receives a factor of $\sqrt{2}$, compared to the SM $q\bar{q}g$ vertex, from the rescaling of the $A_{\mu n}^a$ field:

$$-i\Lambda_{q\bar{q}g^*} = -i\sqrt{2}\Lambda_{q\bar{q}g}, \quad (41)$$

where the 4D strong coupling constant g is related to g_5 by $g \equiv g_5/\sqrt{\pi r}$. Interactions between g 's and g^* 's are somewhat more involved. The cubic interaction terms in the effective 4D Lagrangian density are

$$\begin{aligned} & -i\frac{1}{2}g_5 f^{abc} \int_0^{\pi r} A_\mu^b(x, y) A_\nu^c(x, y) \left[\partial^\mu A^{\nu a}(x, y) - \partial^\nu A^{\mu a}(x, y) \right] dy \\ & = -\frac{1}{2}g f^{abc} \left\{ A_{\mu 0}^{'b}(x) A_{\nu 0}^{'c}(x) \left[\partial^\mu A_0^{'\nu a}(x) - \partial^\nu A_0^{'\mu a}(x) \right] \right. \\ & \quad + 3A_{\mu 0}^{'b}(x) \sum_{n=1}^{\infty} A_{\nu n}^{'c}(x) \left[\partial^\mu A_n^{'\nu a}(x) - \partial^\nu A_n^{'\mu a}(x) \right] \\ & \quad \left. + \frac{1}{\sqrt{2}} \sum_{n,m,\ell=1}^{\infty} A_{\mu n}^{'b}(x) A_{\nu m}^{'c}(x) \left[\partial^\mu A_\ell^{'\nu a}(x) - \partial^\nu A_\ell^{'\mu a}(x) \right] \delta_{\ell,\pm m \pm n} \right\}, \quad (42) \end{aligned}$$

where we introduce the following notation: The Kronecker δ with \pm 's represents the summation over all of the Kronecker δ 's that can be constructed by permuting the $+$ and $-$ signs (*e.g.*, $\delta_{\ell,\pm m \pm n} = \delta_{\ell,m+n} + \delta_{\ell,m-n} + \delta_{\ell,n-m} + \delta_{\ell,-m-n}$). These cubic interaction terms lead to the following Feynman rules for triple vertices involving g 's and g^* 's:

$$\begin{aligned} & -i\Lambda_{g-g_n^*-g_n^*} = -i\Lambda_{g-g-g} \\ & -i\Lambda_{g_n^*-g_n^*-g_{2n}^*} = -i\frac{1}{2}\Lambda_{g-g-g} \\ & -i\Lambda_{g_n^*-g_m^*-g_{|m \pm n|}^*} = -i\frac{1}{2}\Lambda_{g-g-g}, \quad (43) \end{aligned}$$

for $n \neq m$. Similarly, the quartic interaction terms in the effective 4D Lagrangian density are

$$\begin{aligned}
& -\frac{1}{4}g_5^2 f^{abc} f^{ade} \int_0^{\pi r} A_\mu^b(x, y) A_\nu^c(x, y) A^{\mu d}(x, y) A^{\nu e}(x, y) dy \\
& = -\frac{1}{4}g^2 f^{abc} f^{ade} \left[A'_{\mu 0}{}^b(x) A'_{\nu 0}{}^c(x) A'^{\mu d}_0(x) A'^{\nu e}_0(x) \right. \\
& \quad + 6A'_{\mu 0}{}^b(x) A'_{\nu 0}{}^c(x) \sum_{n=1}^{\infty} A'^{\mu d}_n(x) A'^{\nu e}_n(x) \\
& \quad + \frac{2}{\sqrt{2}} A'_{\mu 0}{}^b(x) \sum_{n,m,\ell=1}^{\infty} A'^c_{\nu n}(x) A'^{\mu d}_m(x) A'^{\nu e}_\ell(x) \delta_{\ell, \pm m \pm n} \\
& \quad \left. + \frac{1}{2} \sum_{n,m,\ell,k=1}^{\infty} A'_{\mu n}{}^b(x) A'^c_{\nu m}(x) A'^{\mu d}_\ell(x) A'^{\nu e}_k(x) \delta_{k, \pm m \pm n \pm \ell} \right]. \tag{44}
\end{aligned}$$

The Feynman rules for quadruple vertices involving KK excitations are then

$$\begin{aligned}
& -i\Lambda_{g-g-g_n^*-g_n^*} = -i\Lambda_{g-g-g-g} \\
& -i\Lambda_{g-g_n^*-g_n^*-g_{2n}^*} = -i\frac{1}{\sqrt{2}}\Lambda_{g-g-g-g} \\
& -i\Lambda_{g-g_n^*-g_n^*-g_{|m \pm n|}^*} = -i\frac{1}{\sqrt{2}}\Lambda_{g-g-g-g} \\
& -i\Lambda_{g_n^*-g_n^*-g_n^*-g_n^*} = -i\frac{3}{2}\Lambda_{g-g-g-g} \\
& -i\Lambda_{g_n^*-g_n^*-g_n^*-g_{3n}^*} = -i\frac{1}{2}\Lambda_{g-g-g-g} \\
& -i\Lambda_{g_n^*-g_n^*-g_m^*-g_n^*} = -i\Lambda_{g-g-g-g} \\
& -i\Lambda_{g_n^*-g_n^*-g_m^*-g_{|2n \pm m|}^*} = -i\frac{1}{2}\Lambda_{g-g-g-g} \\
& -i\Lambda_{g_n^*-g_m^*-g_\ell^*-g_{|\ell \pm m \pm n|}^*} = -i\frac{1}{2}\Lambda_{g-g-g-g}, \tag{45}
\end{aligned}$$

for $n \neq m \neq \ell$. The relative coupling strengths are summarized in Fig. 1.

References

- [1] E. Witten, Nucl. Phys. **B471**, 135 (1996); J. Lykken, Phys. Rev. **D54**, 3693 (1996).

- [2] N. Arkani-Hamed, S. Dimopoulos and G. Dvali, Phys. Lett. **B429**, 263 (1998); Phys. Rev. **D59**, 086004 (1999); I. Antoniadis, N. Arkani-Hamed, S. Dimopoulos and G. Dvali, Phys. Lett. **B436**, 257 (1998).
- [3] K.P. Dienes, E. Dudas and T. Gherghetta, Phys. Lett. **B436**, 55 (1998); Nucl. Phys. **B537**, 47 (1999); T. Taylor and G. Veneziano, Phys. Lett. **B212** 147 (1988); D. Ghilencia and G.G. Ross, Phys. Lett. **B442** 165 (1998); hep-ph/9908369; C. Carone, Phys. Lett. **B454** 70 (1999); P. H. Frampton and A. Rasin, Phys. Lett. **B460**, 313 (1999); A. Delgado and M. Quirós, Nucl. Phys. **B559**, 235 (1999); A. Perez-Lorenzana and R. N. Mohapatra, Nucl. Phys. **B559**, 255 (1999); Z. Kakushadze and T. R. Taylor, Nucl. Phys. **B562**, 78 (1999); D. Dumitru and S. Nandi, hep-ph/9906514; K. Huitu and T. Kobayashi, Phys. Lett. **B470**, 90 (1999); H. Cheng, B. A. Dobrescu and C. T. Hill, Nucl. Phys. **B573**, 597 (2000).
- [4] J. Lykken and S. Nandi, Phys. Lett. **B485**, 224 (2000).
- [5] N. Arkani-Hamed, S. Dimopoulos and G. Dvali, Phys. Rev. **D59**, 086004 (1999); V. Barger, T. Han, C. Kao and R.J. Zhang, Phys. Lett. **B461**, 34 (1999); S. Cullen and M. Perelstein, Phys. Rev. Lett. **83**, 268, 1999; L.J. Hall and D. Smith, Phys. Rev. **D60**, 085008 (1999); S.C. Kappadath et. al., BAAS **30** 926 (1998); Ph.D. Thesis, available at <http://wwwgro.sr.unh.edu/users/ckappada/ckappada.html>; D.A. Dicus, W.W. Repko and V.L. Teplitz, Phys. Rev. **D62**, 076007 (2000).
- [6] See, for example: E.A. Mirabelli, M. Perelstein, and M.E. Peskin, Phys. Rev. Lett. **82**, 2236 (1999); G.F. Giudice, R. Rattazzi, and J.D. Wells, Nucl. Phys. **B554**, 3 (1999); T. Han, J.D. Lykken, and R.-J. Zhang, Phys. Rev. **D59**, 105006 (1999); J.E. Hewett, Phys. Rev. Lett. **82**, 4765 (1999); G. Shiu and S.H.H. Tye, Phys. Rev. **D58**, 106007 (1998); T. Banks, A. Nelson, and M. Dine, J. High Energy Phys. **06**, 014 (1999); P. Mathews, S. Raychaudhuri, and S. Sridhar, Phys. Lett. **B450**, 343 (1999); hep-ph/9904232; T.G. Rizzo, Phys. Rev. **D59**, 115010 (1999); C. Balazs, H.-J. He, W.W. Repko, C.-P. Yuan, and D.A. Dicus, Phys. Rev. Lett. **83**, 2112 (1999); I. Antoniadis, K. Benakli, and M. Quirós, Phys. Lett. **B360**, 176 (1999); P. Nath, Y. Yamada, and M. Yamaguchi, *ibid.* **466**, 100 (1999); W.J. Marciano, Phys. Rev. **D60**, 093006 (1999); T. Han, D. Rainwater, and D. Zepfenfeld, Phys. Lett. **B463**, 93 (1999); K. Aghase and N.G. Deshpande, *ibid.* **456**, 60 (1999); G. Shiu, R. Shrock, and S.H.H. Tye, *ibid.* **458**, 274 (1999); K. Cheung and W.Y. Keung, Phys. Rev. **D60**, 112003 (1999).
- [7] I. Antoniadis, Phys. Lett. **B246** 377 (1990).
- [8] E. Accomando, I. Antoniadis, and K. Benakli, Nucl. Phys. **B579**, 3 (2000); A. Datta, P.J. O'Donnell, Z.H. Lin, X. Zhang, and T. Huang, Phys. Lett. **B483**, 203 (2000).

- [9] T.G. Rizzo and J.D. Wells, hep-ph/9906234; C.D. Carone, Phys. Rev. D **61** 015008, 2000.
- [10] M. Masip and A. Pomarol, Phys. Rev. **D60**, 096005 (1999); P. Nath, Y. Yamada and M. Yamaguchi, Phys. Lett. **B466**, 100 (1999); T. G. Rizzo and J. D. Wells, Phys. Rev. **D61**, 016007 (2000).
- [11] A. Delgado, A. Pomarol and M. Quirós, hep-ph/9812489; hep-ph/9911252; A. Pomarol and M. Quirós, hep-ph/9806263; E. Dudas, hep-ph/0006190; M. Masip and A. Pomarol, hep-ph/9902467.
- [12] G.K. Leontaris and N.D. Tracas, hep-ph/9902368 and hep-ph/9908462; M. Bando *et al.*, hep-ph/9906549; I. Antoniadis, K. Benakli, and M. Quirós, Phys. Lett. **B460**, 176 (1999); T.G. Rizzo, hep-ph/9909232; see also Ref. [3]
- [13] H.L. Lai *et al.*, Phys. Rev. **D51**, 4763 (2000).
- [14] J.A.M. Vermaseren, math-ph/0010025.
- [15] M. Masip, hep-ph/0007048.
- [16] F.A. Berends *et al.*, Phys. Rep. **100**, 201 (1983).
- [17] J.M. Cornwall, D.N. Levin and G. Tiktopoulos, Phys. Rev. Lett. **30**, 1268 (1973); Phys. Rev. D **10**, 1145 (1974); D.A. Dicus and V.S. Mathur, Phys. Rev. D **7**, 3111 (1973); B.W. Lee, C. Quigg and H.B. Thacker, Phys. Rev. Lett. **38**, 883 (1977); Phys. Rev. D **16**, 1519 (1977); M. J. G. Veltman, Acta Phys. Polon. **B8**, 475 (1977); C.H. Llewellyn Smith, Phys. Lett. **B46**, 233 (1973).
- [18] C.T. Hill, Phys. Lett. **B266**, 419 (1991); C.T. Hill and S.J. Parke, Phys. Rev. **D49**, 4454 (1994); D.A. Dicus, B. Dutta, and S. Nandi, Phys. Rev. **D51**, 6085 (1995).